This is a **non peer reviewed** pre-print uploaded to EarthArXiv

The manuscript has been submitted to the Geological Society of London

for a Special Issue titled "Tectonic Stress: From the Lithosphere to the

Wellbore" and is currently undergoing peer-review.

Passive Monitoring of *in situ* Stress Using Shear-Wave Splitting: Applications to CO$_2$ Storage and Beyond

Joseph Asplet [*,1], Mark Fellgett [2], Tom Kettlety [1], and J. Michael Kendall [1]

[1]Department of Earth Sciences, University of Oxford, Oxford, UK

[2]British Geological Survey, Nottingham, UK

Wednesday 3rd September, 2025

*Corresponding author: Joseph Asplet joseph.asplet@earth.ox.ac.uk

Abstract

Characterising the *in situ* stress field is important for a range of industrial applciations, such as geological CO_2 storage, geothermal project, hydrocarbon extraction, geological disposal facilities, and for natural seismic hazard assessment. Shear-wave splitting is a passive measurement which can be used to passively monitor changes in the *in situ* stress field. We combine borehole stress and passive seismic data, primarily from microseismicity, across Great Britain to assess the potential of shear-wave splitting to be used to monitor the in situ stress field with several in-depth case studies. At Preston New Road, Lancashire the measured shear-wave splitting fast polarisations, ϕ_f, have a circular mean of $-14°$ and are consistent with the regional S_{Hmax}. At Newdigate, Surrey, the measured shear-wave splitting is best explained by stress-controlled seismic anisotropy, with fast polarisations consistent with regional S_{Hmax} ($\bar{\phi}_f = -51°$) to the north of the Newdigate fault. However, we observed a consistent $90°$ polarisation flip ($\bar{\phi}_f = 40°$) at a station to the south of the fault, which is likely due to overpressured pore fluids. In South Wales there is structure controlled anisotropy from the Neath Disturbance, with ϕ_f measurements near the fault parallel to the fault strike.

These examples demonstrate the potential of shear-wave splitting as a passive measure of *in situ* stress and the challenges that remain. We find that shear-wave splitting, measured from microseismicity, could be used to monitor the *in situ* stress field with sufficient monitoring infrastructure and geological context to constrain interpretations. For

3

CO$_2$ storage projects, incorporating shear-wave splitting into the design of microseismic monitoring networks will enable valuable additional data to be collected.

Key words: Seismic anisotropy, Shear-wave splitting, crustal stress.

Contents

Introduction

The ability to passively characterise the *in situ* stress field in the crust has a range of important applications, such as improving our understanding of tectonic processes, natural hazards, and derisking various industrial subsurface activities. The ability to monitor and assess seal integrity would have applications in any onshore subsurface storage context, such as geological disposal facilities (GDFs) and gas storage, and for geothermal energy. The ability to characterise subsurface stress has important implications for the nascent UK Continental Shelf CO_2 storage industry, as well as continued hydrocarbon extraction. To ensure safe and reliable geological CO_2 storage, new and improved methods are required to monitor the geomechanical response of reservoirs to CO_2 injection (Skurtveit et al., 2022). For these projects, improved spatiotemporal characterisation of the *in situ* stress field could have a significant impact on the operation and containment risk assessment. Many potential offshore CO_2 storage sites in the North Sea require drilling and operating injection wells in regions or formations that may not have been the target of previous hydrocarbon exploration. As a result, there is less data to conduct leakage risk assessments and to construct geomechanical models.

One geophysical observation which can be related to crustal stress is seismic anisotropy. Seismic anisotropy has been studied at various length scales throughout the Earth's crust and mantle using shear-wave splitting. The first measurements of crustal shear-wave splitting were made nearly 45 years ago by Crampin et al. (1980), and shear-splitting has now been

5

observed in local-S throughout the crust and upper mantle (e.g., Teanby et al., 2004a; Gerst and Savage, 2004; Boness and Zoback, 2006; Savage et al., 2010b; Gao et al., 2011; Al-Harrasi et al., 2011; Liu et al., 2014; Stork et al., 2015; Spingos et al., 2023; Hudson et al., 2024b, etc.,).

A common interpretation for seismic anisotropy in the crust, regardless of setting, is the stress-induced alignment of micro-scale fractures (hereafter "stress-induced anisotropy"; Nur and Simmons, 1969; Crampin, 1987; Zatsepin and Crampin, 1997). If the seismic anisotropy observed using shear-wave splitting can be interpreted using this mechanism, then it reveals information on the *in-situ* stress field, particularly the azimuth of the maximum horizontal stress (S_{Hmax} azimuth; e.g., Savage et al., 2010b; Igonin et al., 2022; Guzman et al., 2022; Hudson et al., 2024b). Temporal variations in seismic anisotropy, or shear-wave splitting, can then be used to infer changes in the stress state when sufficient data is available (e.g., Crampin et al., 2015; Stork et al., 2015; Illsley-Kemp et al., 2019; Spingos et al., 2023; Kendall et al., 2025).

In offshore settings, with sufficient microseismic monitoring infrastructure, microseismicity has been used to monitor the stress state for conventional oil and gas reservoirs during extraction (e.g., Teanby et al., 2004a). This raises the potential for shear-wave splitting measured from microseismicity to be used to monitor stress for offshore geological storage projects, such as CO_2 storage projects. The challenge, however, is establishing whether seismic anisotropy can be used as a reliable indicator of *in situ* stress in the upper crust. This assessment requires the input of more traditional stress field characterisation techniques at varying distances from the site. For

6

these reasons, seismic anisotropy should be viewed as an enhancement to stress field characterisation studies.

In this paper, we measure shear-wave splitting for passive seismic data recorded for earthquakes recorded across Great Britain and Ireland from 2010 to 2022. This new shear-wave splitting dataset allows for an assessment of the relationship between crustal seismic anisotropy and the S_{Hmax} azimuth measured using other methods in a range of settings.

Shear-wave splitting has been previously measured for teleseismic core-refracted shear-wave phases, which predominately sample seismic anisotropy in the mantle, recorded by seismometers in the United Kingdom (Helffrich, 1995; Bastow et al., 2007). However, there has been no complete study of crustal shear-wave splitting across the United Kingdom. The UK is relatively well instrumented, with the British Geological Survey operating a permanent seismic network of 47 broadband seismometers across the British Isles (Baptie, 2021). This allows us to investigate shear-wave splitting for a range of settings, using both industrial and natural microseismicity. In addition, there are 474 S_{Hmax} azimuth observations from borehole data available across Great Britain which are used to validate the results ((Kingdon et al., 2022)). Where there are fewer observations of S_{Hmax} azimuth, for example in the South of England, new stress field observations were interpreted from dual caliper logs (Fellgett and Williams, 2025). We use this joint dataset of shear-wave splitting and stress data to highlight the potential of shear-wave splitting studies to passively monitor *in situ* stress, the challenges that remain, and the potential pitfalls for monitoring network designs.

7

Seismic Anisotropy

Seismic anisotropy is the variation in seismic velocity, in our case shear-wave velocity, with propagation direction. Seismic anisotropy in the Earth's crust can occur due to various mechanisms operating at different length scales. This can range from the preferential alignments of mineral grains (or crystal preferred orientation, CPO) within a rock formation, to the alignment of heterogeneities, such as sedimentary layering (Backus, 1962) or fracture sets (e.g., Hudson, 1981; Chapman, 2003; Jin et al., 2018), which are smaller than the sampling seismic wavelength. Despite the wide variety of potential mechanisms, one unifying trait is that they are all expressions of order in materials.

In the crust, one of the most commonly observed mechanisms for seismic anisotropy is microscale fractures aligned with the maximum horizontal stress (S_{Hmax}) azimuth (e.g., Teanby et al., 2004a; Boness and Zoback, 2006; Savage et al., 2010b; Gao et al., 2011; Al-Harrasi et al., 2011; Stork et al., 2015; Illsley-Kemp et al., 2019; Hudson et al., 2024b). This is because most passive seismic observations are for vertical or sub-vertically propagating shear-waves which are not sensitive to seismic anisotropy due to sedimentary layering, which typically develops with a vertical symmetry axis (also know as vertical transverse isotropy, VTI). When saturated with a fluid (such as meteoric water, hydrocarbons, supercritical CO_2, or melt), these aligned microcracks produce a strong seismic anisotropy (Hudson, 1981; Chapman, 2003). When differential horizontal stresses are applied to a rock, this causes microscale cracks in a rock to preferentially

8

open or close such that the total fracture set aligns with the maximum horizontal stress (Crampin, 1999). For this anisotropy to be observed by shear-wave splitting, the microcracks must develop, on average, near-vertically. Therefore, this seismic anisotropy will only develop at depths where where the vertical stress exceeds the magnitude of the minimum horizontal stress, i.e., in normal and strike slip faulting environments. This dependence of seismic anisotropy on differential horizontal stresses can be described by the anisotropic poroelasticity model (APE; Zatsepin and Crampin, 1997; Crampin and Zatsepin, 1997). Seismic anisotropy due to aligned, fluid-filled microcracks is also dependent on the fracture properties. Microcrack density and aspect ratio are the primary parameters that control the strength of anisotropy for an aligned fracture set (Hudson, 1981; Chapman, 2003). APE predicts that increasing differential horizontal stresses increases the aspect ratio and density of the aligned microcracks, and therefore the strength of seismic anisotropy (Zatsepin and Crampin, 1997; Crampin, 1999). Furthermore, under the APE model the aspect ratio and orientation of the microcracks are sensitive to small variations in the azimuth and magnitude of the horizontal stress field (Zatsepin and Crampin, 1997; Crampin and Zatsepin, 1997; Crampin, 1999). This makes seismic anisotropy, in theory, sensitive to the azimuth and magnitude of the horizontal stress field.

Rock physics models that incorporate poroelastic squirt – where seismic waves compress compliant cracks more than stiff pores resulting in a flow of pore fluids between cracks of different orientations (e.g., Chapman, 2003; Jin et al., 2018) – show that along with microcracks, meso-scale

fractures (i.e., fracture significantly larger than the grainsize) control the seismic anisotropy. This makes the seismic anisotropy frequency-dependent. Where frequency-dependent anisotropy is observed, it is then possible to invert for fracture size and density, which is a useful tool when characterising a reservoir and assessing seal integrity (Al-Harrasi et al., 2011). Another consequence of squirt flow models is that the fluid filled fractures may also induce attenuation anisotropy (Carter and Kendall, 2006; Asplet et al., 2024) which can affect shear-wave splitting measurements (Asplet et al., 2024), but also offers the potential to further constrain fracture properties. Here, we do not consider frequency-dependent anisotropy or attenuation anisotropy and refer to microcracks and meso-scale fractures collectively as 'cracks'.

Stress induced anisotropy is not, however, the only mechanism for seismic anisotropy widely observed in the Earth's crust. In many settings, stress-induced anisotropy is not observed, or is overprinted by the effect of structural features, particularly large fault zones where anisotropic fabrics due to cracks or fault damage zones are aligned with fault strike and not S_{Hmax} (e.g., Boness and Zoback, 2006; Hurd and Bohnhoff, 2012; Liu et al., 2014; Jiang et al., 2021; Okada et al., 2024). However in some settings, tectonic features appear to have little-to-no impact on the observed anisotropy (Spingos et al., 2023). It is also possible for multiple fracture sets to develop, which creates an anisotropic fabric that is not completely stress-dependent (Baird et al., 2013). In collisional tectonic settings, seismic anisotropy can develop due to CPO in terranes and the mantle wedge (e.g., Okaya et al., 2016; Lynner et al., 2024), where in higher

temperature conditions crystalline rocks undergo plastic deformation. The resulting anisotropic crystal fabric preserves the strain orientation.

Shear-wave splitting

Shear-wave splitting, or seismic birefringence, occurs when an incident shear-wave propagates through an anisotropic medium. Upon entering the medium the shear-wave is split in two, where one of the shear-waves is polarised along the fast velocity direction, or the fast polarisation direction ϕ_f, and the other along an (assumed) orthogonal direction. As shear-wave splitting is typically measured at the seismic station for sub-vertically incident shear-waves, ϕ_f is reported in the geographic reference frame as an azimuth from north. It should be noted that ϕ_f is reported in the range $-90°$ to $90°$ as the polarisations have a $180°$ symmetry. The two shear-waves, referred to as the fast (or S_1) and slow (or S_2) shear-waves, propagate through the anisotropic medium at different velocities (Figure 1). This introduces a time delay between the two shear-waves, δt. This time delay depends on both the thickness of the anisotropic medium and the strength of the seismic anisotropy. When studying local shear-wave splitting, it is important the note that δt is accumulated along the entire ray path. Therefore, δt may vary with earthquake depth, depending on the thickness of the anisotropic medium. To interpret δt, and to search for signal of depth-varying anisotropy, this effect must be account for. Here we convert delay time δt to percent anisotropy, ξ, where

$$\xi = 100(V_S * \frac{\delta t}{d}) \, , \tag{1}$$

11
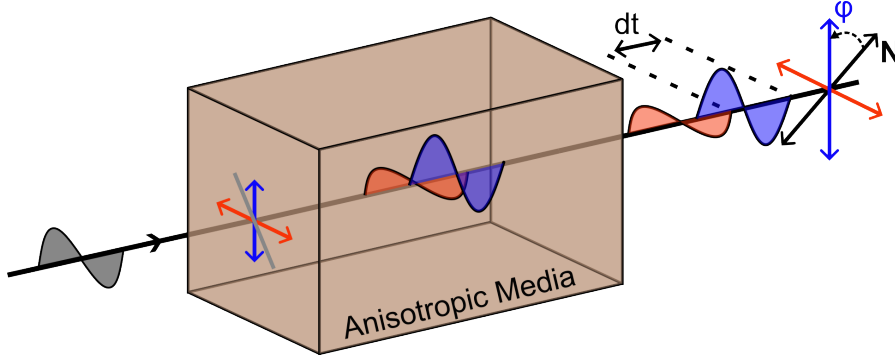
Figure 1: A schematic view of shear-wave splitting. The incident shear-wave encounters an anisotropic medium and is split into a fast (blue) and slow (red) shear-wave which are sub-orthogonally polarised. The splitting is preserved along the remainder of the ray path and parameterised in terms of the fast polarisation direction ϕ (typically measured relative to North, but can also be measured in the ray reference frame) and the delay time δt between the fast and slow shear-waves.

where V_S is an assumed mean shear-wave velocity and d is the ray path length, assuming a straight ray from source to receiver.

For seismic anisotropy due to aligned sub-vertical fractures, rock physics models predict that the measured ϕ_f (in the geographic reference frame) will be aligned with the fracture strike (Hudson, 1981; Chapman, 2003). The APE model of microcrack growth under triaxial differential stresses predicts that microcracks, and therefore ϕ_f, will preferentially orient with S_{Hmax} (Zatsepin and Crampin, 1997). This allows for measurements of ϕ_f to be used to infer S_{Hmax} azimuth. This framework is what allows shear-wave splitting to be used to interpret variations in S_{Hmax} azimuth in settings ranging from volcanoes (e.g., Gerst and Savage, 2004; Bianco et al., 2006; Savage et al., 2010b; Baird et al., 2015; Illsley-Kemp et al., 2019), to industries such as hydraulic fracturing (e.g., Baird et al., 2013; Igonin et al., 2022), CO_2 injection (e.g., Stork et al., 2015), and hydrocarbon

reservoirs (e.g., Angerer et al., 2002; Teanby et al., 2004a; Kendall et al., 2007). Theoretically, temporal variations in δt, or anisotropic strength, are sensitive to variations in the magnitude of horizontal stresses. In the case where pore fluids are highly pressurised, a $90°$ flip in ϕ_f may occur (Zatsepin and Crampin, 1997). These polarisation flips have been observed at the field scale (e.g., Angerer et al., 2002; Teanby et al., 2004a) and, when observed, could provide constraints on *in situ* pore fluid pressures.

The advantage of shear-wave splitting is that, with sufficient instrumentation, measurements can be made at significantly higher spatial and temporal resolutions than borehole measurements of stress, such as borehole breakout analysis and drilling-induced tensile fractures. Shear-wave splitting is also independent from borehole measurements, and gives the potential to fill gaps between boreholes to provide a higher-resolution image of the subsurface stress field. Where there is sufficient data, either due to a large number of earthquakes, stations, or both, shear-wave splitting tomography (e.g., Abt and Fischer, 2008; Johnson et al., 2011; Kufner et al., 2023), or spatial averaging (e.g., Johnson et al., 2011; Pastori et al., 2019; Spingos et al., 2023) can be used to map seismic anisotropy and, therefore, S_{Hmax} in the correct setting, across a region. Temporal variations in shear-wave splitting can also be used to infer changes in regional stress during earthquake sequences (Crampin et al., 2002; Volti and Crampin, 2003; Pastori et al., 2019), volcanic activity (e.g., Bianco et al., 2006; Kendall et al., 2025), and industrial activity (e.g., Teanby et al., 2004a). It has been suggested that these stress-induced temporal variations in seismic anisotropy could enable forecasting of earthquakes (e.g., Crampin

et al., 1999; Crampin et al., 2008, etc.,) with Crampin et al. (1999) reporting a successful "stress forecast" of a M 5.0 earthquake in Iceland. Subsequent statistical analysis has questioned this result (Seher and Main, 2004) and it has proved challenging to achieved similar forecasts outside or retrospective analysis (Crampin et al., 2015). In complex tectonic environments, temporal variations in shear-wave splitting do not uniformly occur in response to earthquakes, with a review of data in the Eastern Gulf of Corinth showing that some of the largest events in the thirteen year catalogue for region had no effect on the measured shear-wave splitting (Spingos et al., 2023).

Measurements of shear-wave splitting have also been successfully inverted for fracture properties, such as strike, dip, fracture radius, and density (e.g., Verdon and Kendall, 2011; Al-Harrasi et al., 2011). Inversion of shear-wave splitting data directly for anisotropic fabrics is still a nascent field. Recent developments have primarily focused on studying mantle anisotropy (e.g., Wookey, 2012; Asplet et al., 2023; Link and Long, 2024), however frameworks have also been previously developed for reservoir-scale inversions to identify vertically aligned fractures and horizontal sedimentary fabrics using fracture compliances (Verdon et al., 2009). Future work may allow for these methods to be applied to measurements of local shear-wave splitting, and extended to invert measurements directly for differential horizontal stresses using the APE model.

14

Measuring shear-wave splitting

If there is no seismic anisotropy, and therefore shear-wave splitting, along the ray path a shear-wave arrival will be recorded with an approximately linear particle motion. If shear-wave splitting has occurred then the phase shift due to δt will produce an elliptical particle motion. Detecting and then correcting for this elliptical particle motion underpins most methods for measuring shear-wave splitting. Here we use eigenvalue minimisation (Silver and Chan, 1991; Walsh et al., 2013), which is a widely used method for measuring shear-wave splitting that can be automated. Shear-wave splitting parameters can also be measured using other methods such as cross-correlation (Bowman and Ando, 1987), or shear-wave splitting can be measured as a scalar splitting intensity (Chevrot, 2000). Recent work has demonstrated that there could be potential for deep learning methods to be used to measure shear-wave splitting, but there is currently insufficient labelled training data to train a model and further work is needed on establishing uncertainty estimates from neural networks (Chakraborty et al., 2024).

There are now numerous software packages now available for measuring shear-wave splitting, with implementations available in most modern programming languages (Table 1). Modern implementations are mainly based on the eigenvalue minimisation method (Silver and Chan, 1991; Walsh et al., 2013), with the primary considerations on the choice of software to use being the preference of the researcher in terms of measurement strategy, such as the level of automation, method used to

15

Software	Authors	Language	GUI	Automation level
MFAST	Savage et al. (2010a)	MATLAB	No	Automated
SHEBA	Wuestefeld et al. (2010)	Fortran	No	Manual
Pytheas	Spingos et al. (2020)	Python	Yes	Manual and Automated modes
SplitLab	Wüstefeld et al. (2008)	MATLAB	Yes	Semi-automated
SplitRacer	Reiss and Rümpker (2017)	MATLAB	Yes	Semi-automated
SplitPy	Audet and Schaeffer (2019)	Python	Yes	Manual and Automated modes
SWSPy	Hudson et al. (2023)	Python	No	Automated

Table 1: Comparison of commonly used shear-wave splitting software packages. Many shear-wave splitting codes exist with various levels of developer support, this table aims to capture those which are more commonly used and is not intended to be a full compilation of available codes.

choose the optimum analysis window, and quality control results.

Here shear-wave splitting is measured using SHEBA (Wuestefeld et al., 2010), a Fortran shear-wave splitting code. All waveforms are uniformly bandpass filtered between $1\,\mathrm{Hz}$ and $20\,\mathrm{Hz}$. For each candidate event-station pair the waveforms are manually inspected and analysis window start/end ranges are picked, with cluster analysis used to pick the optimum window following Teanby et al. (2004b). For the optimum analysis window we (Figure 2) grid search over candidate shear-wave splitting parameters to find the best fitting $\phi_f, \delta t$. Fast polarisations in the range $-90° \leq \phi_f \leq 90°$ are used, with a parameter range in δt chosen depending on the expected strength of anisotropy and frequency content of the shear-waves. Here we use $0\,\mathrm{s} \leq \delta_t \leq 0.1\,\mathrm{s}$. For each set of splitting parameters the input waveforms are corrected for the shear-wave

16

splitting described by those parameters, and the trace covariance matrix in computed where the first and second eigenvalues, λ_1 and λ_2, represent the horizontal components (Silver and Chan, 1991; Walsh et al., 2013). The ratio $\frac{\lambda_2}{\lambda_1}$ describes the linearity of the particle motion, where $\lambda_2 = 0$ for linear particle motion. The eigenvalue minimisation method seeks to minimise λ_2 and restore linear particle motion. Uncertainties in the measured splitting parameters are estimated using the F-test

$$\lambda_2^{0.95}(\phi, \delta t) = \lambda_{2_{min}}\{1 + [k/(v - k)]F_{k,v-k}^{0.05}\}, \tag{2}$$

where $k = 2$, the number of estimated splitting parameters, v is the estimated degrees of freedom of the data and $F_{k,v-k}$ is an F-distribution (Silver and Chan, 1991; Walsh et al., 2013).

The Shear-wave Window

Before making a measurement, it is important to ensure that the chosen shear-wave is within the shear-wave window. Shear-waves particle motions are modified by interactions with a free surface (Nuttli, 1961), which makes it difficult to accurately measure shear-wave splitting. To avoid this effect, the shear-waves' ray path must have an incidence angle at the free surface which is less than the critical angle (Booth and Crampin, 1985). The most common assumption, which we follow here, is a critical angle, or shear-wave window, of $45°$. This assumes that low velocity layers near the surface will turn incident shear-wave ray paths such that they are near-vertical at the free surface. To avoid shear-wave window affects on our measurements, all data where the earthquake epicentral distance from

17

a receiver is less than or equal to its depth is discarded.

Measurement Quality Control

Measurements are then subjected to quality control processes. Initially quality codes are assigned automatically using the estimated measurement uncertainty as shown in Table 2, where the uncertainty thresholds for ϕ have been chosen to match the uncertainties in S_{Hmax} azimuth associated with the different stress data quality codes used by the World Stress Map (Heidbach et al., 2016).

Quality Code	σ_ϕ	$\sigma_{\delta t}$
A	$\leq 15°$	$\leq 0.005\,\mathrm{s}$
B	$\leq 20°$	$\leq 0.01\,\mathrm{s}$
C	$\leq 25°$	$\leq 0.015\,\mathrm{s}$
D	$\leq 40°$	$\leq 0.03\,\mathrm{s}$
E	$> 40°$	$> 0.03\,\mathrm{s}$

Table 2: Measurement uncertainty thresholds used to assign data quality codes. Quality A-C data is then manually reviewed to ensure a clear split

Measurements are then manually inspected to validate this automatic quality control. Input waveforms, selected shear-wave window, corrected waveforms and eigenvalue minimisation surface (Figure 2) are inspected to ensure a good shear-wave splitting result has been achieved. This inspection process is important as crustal shear-wave splitting measurements commonly suffer from cycle skipping, where one shear-wave is pushed outside the measurement window, which artificially reduces the eigenvalue ratio and the estimated measurement uncertainties.

18

Cycle Skipping

Cycle skipping, where waveforms are mismatched by more than one half-cycle, is a persistent problem for local shear-wave splitting studies. If the cycle skipping is of one half-cycle then the fast and slow shear-waves can be interchanged resulting in a $90°$ flip in fast polarisation, a $T/2$ shift in δt, where T is the shear-wave period. Cycle skipping has been shown to affect measurements of the shear-wave source polarisation (e.g., Matcham et al., 2000; Walsh et al., 2013). Skipping of multiple cycles can also occur if the chosen analysis window is too short relative to the maximum delay time, where $\frac{\lambda_2}{\lambda_1}$ is minimised by shifting one of the shear-waves out of the measurement window. Such a measurement is characterised by a delay time near the maximum value permitted in the grid search. Selecting larger analysis windows can partially mitigate this issue, but then has the drawback of polluting the measurement windows with additional noise or secondary arrivals.

A modification of the window cluster analysis method of Teanby et al. (2004b) can be used to screen cycle skipping somewhat effectively, as these measurements will exhibit clusters at 90 degree or half-cycle intervals (Savage et al., 2010a; Castellazzi et al., 2015). Manual screening, however, is the most reliable, albeit time-consuming, way to ensure measurements effected by cycle skipping are removed. As the majority of the shear-wave splitting measured here is for previously unstudied regions, manual inspection of measurements is already warranted to ensure data quality. Where cycles skipping is found, the analysis windows are adjusted and

19

measurements repeated, if cycle skipping persists the shear-wave splitting measurement is rejected.

Null Measurements

If the incident, un-split, shear-wave is already polarised in the fast or slow directions of the medium, or there is no anisotropy in the plane of the shear-wave particle motion, then no shear-wave splitting occurs (e.g., Silver and Chan, 1991; Wuestefeld et al., 2010). This is known as a "null" measurement, and they must be treated separately to measurements of shear-wave splitting. Nulls can be detected both by using automated methods (Savage et al., 2010a; Wuestefeld et al., 2010), and by data inspection. Whilst automated methods are necessary for large data sets they can result in misclassification of split waveforms as 'null'. In studies of the Earth's mantle, nulls can give important insights (e.g., Asplet et al., 2020), but here we discard null measurements in line with other studies (e.g., Johnson et al., 2011; Castellazzi et al., 2015; Pastori et al., 2019, etc.,).
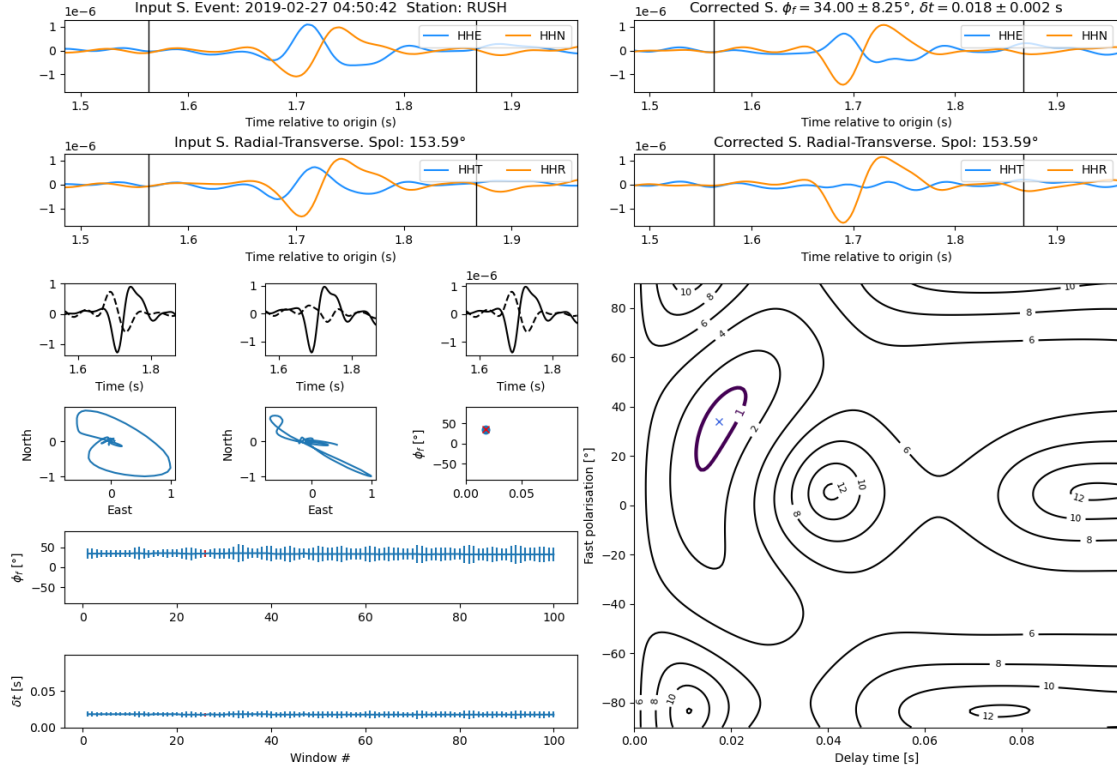
Figure 2: Example diagnostic output plot for a shear-wave splitting measurement made at the station RUSH for a M_L -1.1 earthquake which occurred at 2019-02-27 04:50:42 UTC. After manual inspection this measurement is categorised as an 'A' or highest quality measurement. Top panels show the input (top left) and corrected (top right) shear-wave phase, where the vertical black bars show the optimum analysis window. The second row shows in the input and corrected waveforms rotated to the measured source polarisation direction. The third row shows the normalised input and corrected waveforms, along with the unnormalised, corrected waveforms. The fourth row shows particle motion plots, which shows the North and East component waveforms plotted against each other, for the input and corrected waveforms, along with the measured fast polarisation (ϕ_f) and delay time (δt) for each window used in the cluster analysis of (Teanby et al., 2004b). Lower panels show ϕ_f and δt plotted against window number. The contour plot on the lower right shows $\frac{\lambda_2}{\lambda_1}$ calculated at each ϕ_f, δ_t for the optimum analysis window. Blue cross shows the best fitting shear-wave splitting parameters, the bold contour shows the 95% confidence region. $\frac{\lambda_2}{\lambda_1}$ is also normalised by the 95% confidence value. Other example measurements are included in the supplementary material.

Data Used

Across the UK the British Geological Survey maintain a network of 47 permanent broadband seismic stations (GBarray, network code GB; British Geological Survey, 1970), complemented by temporary deployments of 34 broadband seismometers in the North of England (UKarray, network code UR; British Geological Survey, 2015) and five near Newdigate, Surrey during our study period of 2010 to 2022 (Baptie, 2021). There are 3079 earthquakes earthquakes recorded in the BGS earthquake catalogue between 2010 and 2022 (British Geological Survey, 2025). Despite the large number of events many are unsuitable for shear-wave splitting because of data embargoes or no S phase was picked. When these events are disregarded the dataset is reduced to 1452 viable candidate earthquakes for shear-wave splitting analysis.

The shear-wave window restriction (see Section "The Shear-wave Window") reduces dataset from 1452 earthquakes to 377 earthquakes where shear-wave splitting measurements can be made (Figure 3). The focal depths and reported local magnitudes of all earthquakes considered, and those where shear-wave splitting can be measured are summarised in Figure 4. This pronounced ca. 75% reduction in our initial dataset is due to the previously described shear-wave window effect. Whilst Great Britain is well instrumented the seismic network is sparse relative to epicentral distances required for seismicity to lie within the shear-wave window. The mean focal depth of earthquakes recorded in the BGS catalogue from 2010 − 2022 is $6.34\,\mathrm{km}$ and 80% of earthquakes have a focal depth under $10\,\mathrm{km}$ (Figure 4a).

The shear-wave window imposes a significant geographical heterogeneity, which limits our ability to compare shear-wave splitting and stress across the the UK. However, the sites where data are available are data rich and are good analogues for deployments which could be used to assess *in situ* stress for sites of interest. The majority of the 377 events where shear-wave splitting can be measured are recorded by three temporary deployments. Two of these deployments were the surface monitoring stations for Stages 1 and 2 of hydraulic fracturing at Preston New Road, Lancashire (Clarke et al., 2019b; Kettlety et al., 2020) and the other targeted an earthquake swarm near Newdigate, Surrey (Hicks et al., 2019). Similar temporary monitoring networks are used to monitor onshore microseismicity for a variety of geological storage activities and hydraulic fracturing (e.g., Kaven et al., 2015; Verdon et al., 2016; Goertz-Allmann et al., 2024).

**Preston New Road, Lancashire**

In 2018 and 2019, hydraulic fracturing took place on two horizontal wells drilled in Northwest England. This was part of efforts to assess and extract shale gas by Cuadrilla Resources Limited. The project was located around $3\,\mathrm{km}$ east of the town of Blackpool. Two horizontal wells were drilled into the Bowland Shale at the Preston New Road site. The first well, PNR-1z, was stimulated in late 2018 and the second well, PNR-2, was stimulated in August 2019. Shortly before, during, and for some months after injection, microseismic monitoring was conducted by the operator. Independent monitoring was also done by the British Geological Survey. The temporary seismic monitoring networks consisted of three-component

short period and broadband sensors recorded hundreds of events in the two periods of hydraulic fracturing. We measure shear-wave splitting using earthquakes recorded in the British Geological Survey catalogue, along with further microseismic events recorded at the broadband surface stations at Preston New Road (Clarke et al., 2019b; Kettlety et al., 2020). This gives an initial dataset of 380 earthquakes which is reduced to 140 after filtering of earthquakes outside the shear-wave window (Figure. Earthquakes used have depths ranging from $1.6\,\mathrm{km}$ to $2.9\,\mathrm{km}$ and local magnitudes in the range $-1.7 \leq \mathrm{M_L} \leq 2.9$. The station codes used for the surface monitoring network changed from IOXX to PNRXX between the stimulation of PNR-1z and PNR-2, but the locations and type of sensors at each location remained consistent. The continuous waveform data from this monitoring effort is now publicly available for study.

Newdigate, Surrey

In April 2018, a swarm of earthquakes began near the town of Newdigate in Surrey. In July (HORS, RUSH) and August (GATW, STAN, BRDL) 2018 a temporary network of broadband seismometers was deployed to monitor the seismicity (Hicks et al., 2019). In May 2019 the station GATW was removed and was replaced in June 2019 by another station near Gatwick (GAT2). The British Geological Survey recorded 34 earthquakes prior to the installation of the monitoring network, with a further 135 earthquakes recorded after 12 July 2018, for a total of 168 earthquakes recorded in the swarm. Figure 6 shows the locations of earthquakes recorded in the swarm and the locations of the monitoring stations. Despite occurring close to

onshore hydrocarbon wells, it was quickly shown that the Newdigate swarm was likely a natural earthquake swarm associated with tectonic reactivation along a pre-existing E-W striking fault in the Weald Basin (Hicks et al., 2019). The seismicity is shallow, with focal depths ranging from $2\,\mathrm{km}$ to $3.6\,\mathrm{km}$ and a mean depth of $2.3\,\mathrm{km}$. Earthquake local magnitudes were in the range $-1.6 \leq M_L \leq 3.1$, with the majority of events being microseismic with $M_L \leq 2$ (Hicks et al., 2019).
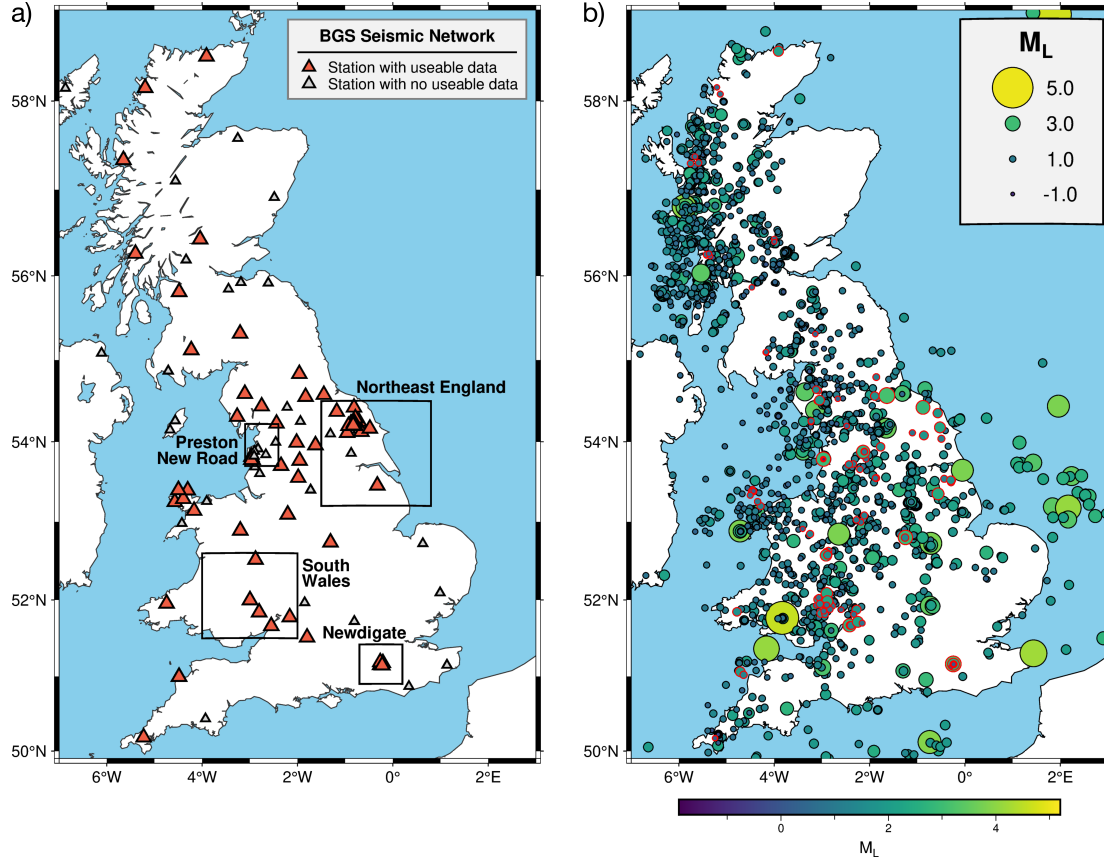
Figure 3: Map showing earthquakes and seismic stations used in this study. Panel (**a**) shows the locations of seismometers operated by the British Geological Survey in the UK from 2010 to 2022 for which waveform data is publicly available. Seismometers that recorded events considered viable candidates for this study are shown in red, with the broadband seismometers operated by the BGS shown in grey. Also shown are the regions studied in this paper. Panel (**b**) shows earthquakes recorded by the BGS from 2010 to 2022 (British Geological Survey, 2025). Earthquakes are sized and coloured by local magnitude. Earthquakes which are within the shear-wave window of a station where a S pick has been made are considered viable shear-wave splitting candidates and are enclosed in red circles. Earthquakes which are not considered viable candidates are enclosed by black circles.
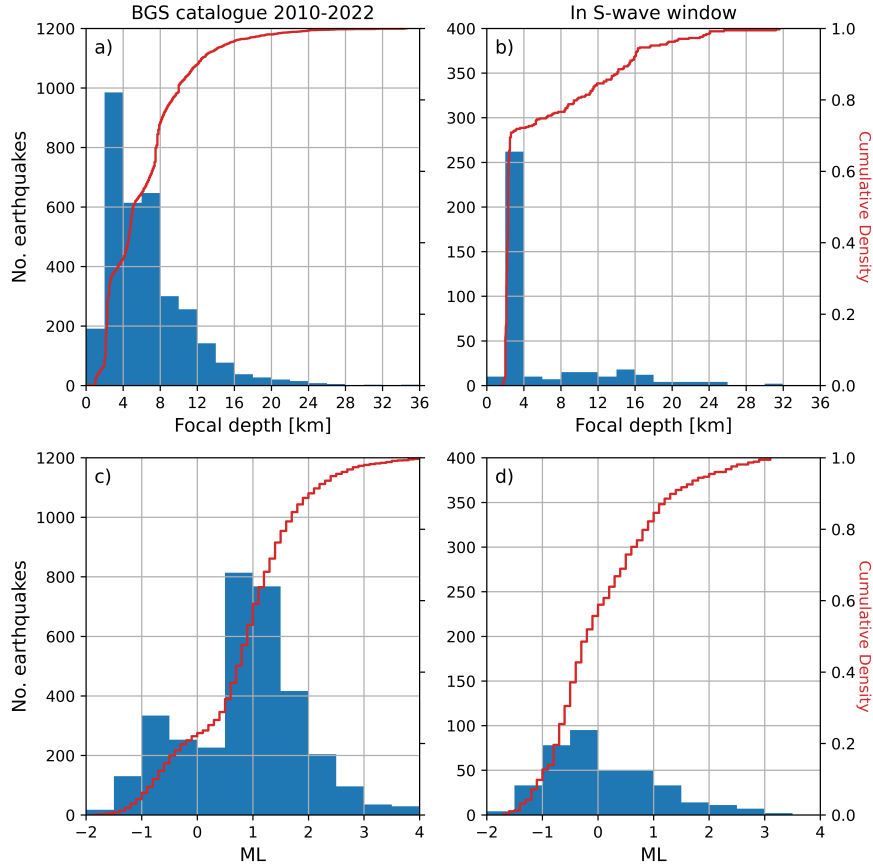
Figure 4: Histograms showing the focal depth (**a**) and local magnitude (**c**) of all earthquakes compiled in this study and for the dataset of 959 earthquakes which are viable for shear-wave splitting analysis in this report (**b,d**). For each panel, empirical cumulative density functions are calculated and are shown by the red line.
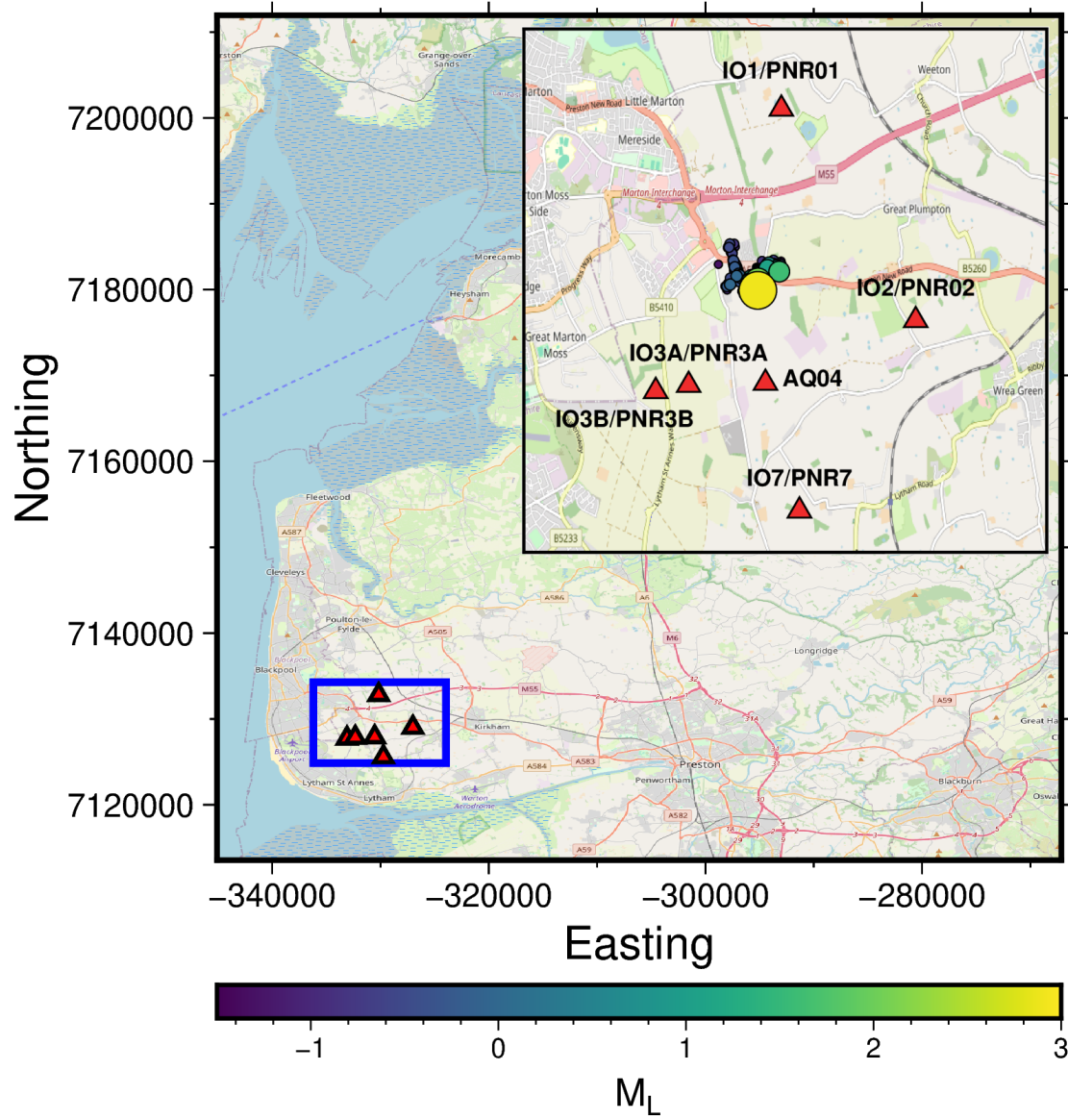
Figure 5: Map showing the Preston New Road study region and the location on the surface monitoring stations used (red triangles). Inset map shows the earthquakes recorded by the surface monitoring stations, coloured and size by the reported earthquake magnitude (Clarke et al., 2019b; Kettlety et al., 2024). Station codes for the surface monitoring stations are also shown with the codes for some monitoring stations changing from IOXX to PNRXX between the stimulation of PNR-1z and PNR-2, but the locations and type of sensors at each location remained consistent. Background map data is taken from OpenStreetMap (OpenStreetMap contributors, 2017).
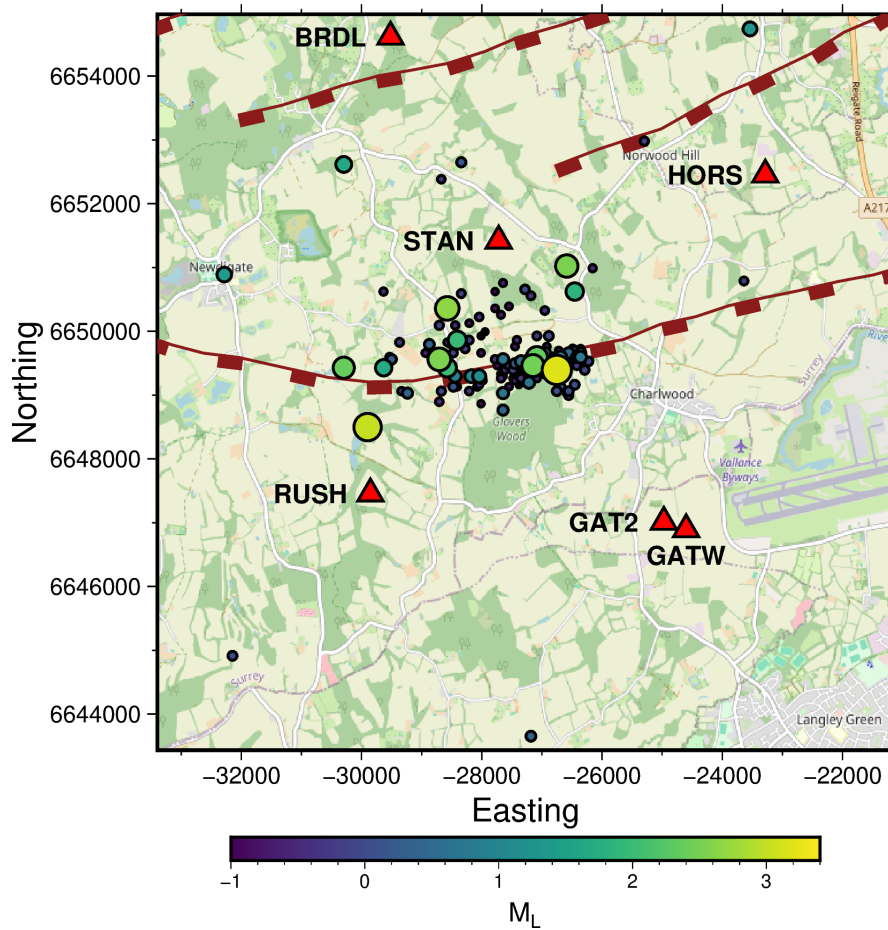
Figure 6: Map showing the Newdigate earthquake swarm using event relocations from Hicks et al. (2019). Earthquakes are sized and coloured by local magnitude (M_L). Monitoring stations are shown by the red triangles. Background map data taken from OpenStreetMap (OpenStreetMap contributors, 2017).

Stress data

In order to ground truth the stress orientations from the shear wave splitting a comparison should be made to existing stress field orientations. For the UK the primary existing source of stress field data for the British Isles is the Stress Map of Great Britain and Ireland 2022 (Kingdon et al., 2022). This dataset comprises 474 data points obtained from a variety of sources including: earthquake focal mechanisms; borehole breakouts, overcoring and hydraulic fracturing tests which have been ranked based on their reliability to assess regional stress field orientation (Heidbach et al., 2018). Here we only use the 154 data points with a quality code A, B, or C (Figure 7a), which indicates the data has an uncertainty in S_{Hmax} orientation of $\pm15°$, $\pm20°$ or $\pm25°$ respectively.

Across much of the UK the dominant orientation of S_{Hmax} is NW/SE though there are significant regional variations (Figure 7a; Heidbach et al., 2018; Kingdon et al., 2022). The 2022 stress field data does constrain S_{Hmax} azimuth across most of the UK, however there are no existing data points in the Weald near Newdigate. To confirm the regional S_{Hmax} azimuth in the Weald, borehole breakout analysis was undertaken on logs for six boreholes (Fellgett and Williams, 2025). The analysis was based on dual-caliper logs using the methodology detailed in (Heidbach et al., 2016). For more information on the use of calipers to determine in-situ stress orientations please see: Bell and Gough (1979), Plumb and Hickman (1985), and Heidbach et al. (2016).
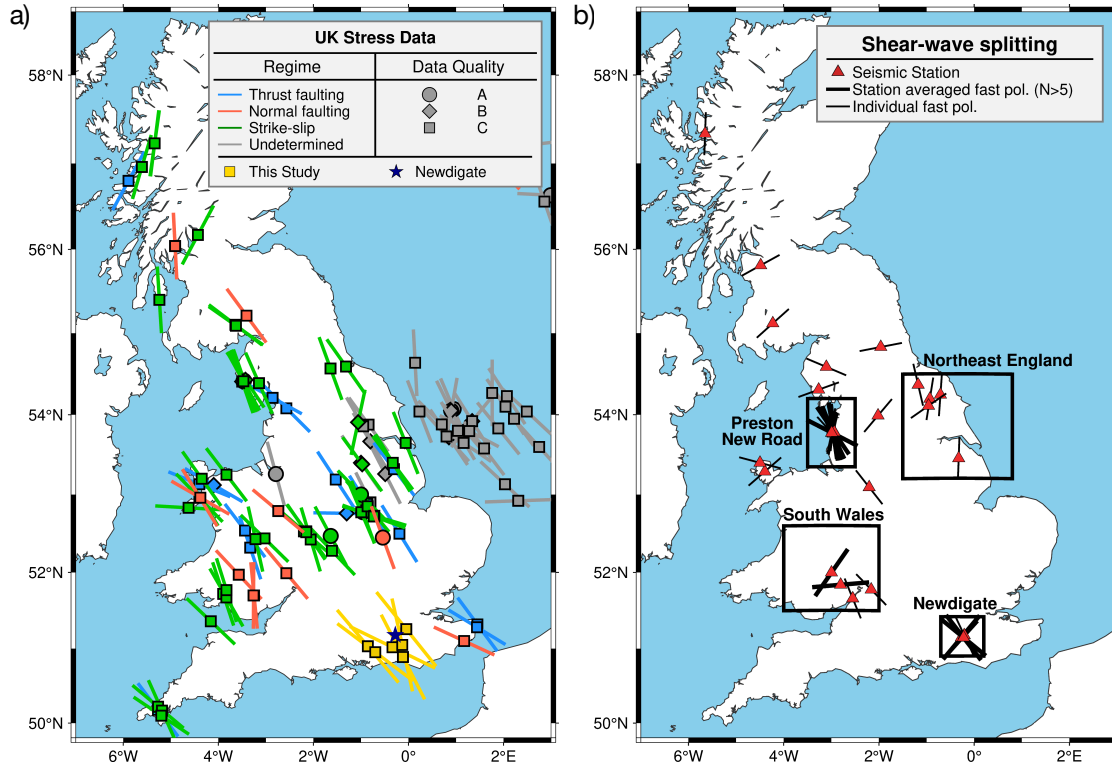
Figure 7: Maps shows the stress (**a**) and shear-wave splitting data **b** used. Panel **a** shows the stress data used in this study plotted as bars oriented with the interpreted S_{Hmax}. The majority of the data is taken from the Stress Map of Great Britain and Ireland 2022 (Kingdon et al., 2022), these datapoints and bars are coloured to indicate interpreted tectonic regime. Stress data from this study for the Weald Basin is coloured gold (Fellgett and Williams, 2025). Symbols are drawn at the measurement location and correspond to data quality as defined by the World Stress Map (Heidbach et al., 2016) for data of quality A (circle), B (diamond), or C (square). Panel (**b**) shows the 320 quality A – C shear-wave splitting measurements. Shear-wave splitting measurements are plotted as bars located at the earthquake-station midpoint where the bar orientation shows the measured fast polarisation direction and bar length is proportional to δt. Where five or more measurements have been made at a single station, the station averaged shear-wave splitting is shown instead. Regions where comparison between shear-wave splitting measurements and World Stress Map data can be made are shown in boxes.
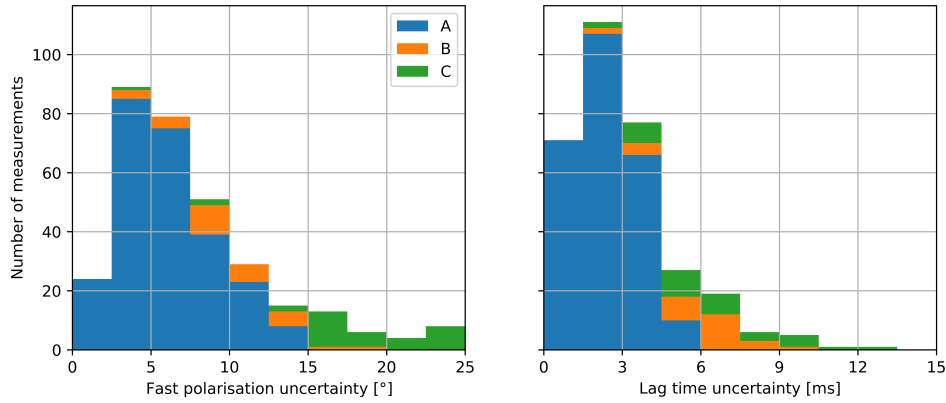
Figure 8: Stacked histograms of measurement uncertainties in ϕ_f (**a**) and δt (**b**) for the 320 quality A to C splitting measurements made across the UK. See text for criteria used for different data quality codes.

Results

Shear-wave splitting is measured for the identified 377 candidate earthquakes at all suitable stations, resulting in 886 measurements. Analysis is restricted to the 320 measurements classified as quality A, B, or C (Table 2), where the measured shear-wave splitting clear enough to allow for interpretation. The vast majority of this data, 254 measurements, are quality A (Figure 8). The data attrition, with 36% of measurements of sufficient quality to interpret, is due to noisy waveform data, the previously described issue of cycle skipping, and the exclusion of 50 null measurements. This level of data attrition is in line with previous shear-wave splitting studies (e.g., Teanby et al., 2004a; Pastori et al., 2019). A table of all shear-wave splitting results is available in the supplementary material.

The shear-wave splitting results can be grouped into four regions: Preston New Road, Newdigate, South Wales, and Northeast England (Figure 7b). For each region aggregate rose histograms of fast polarisation direction are made, with a bin width of $10°$ (Figure 9). In each region we also aggregate available stress data.
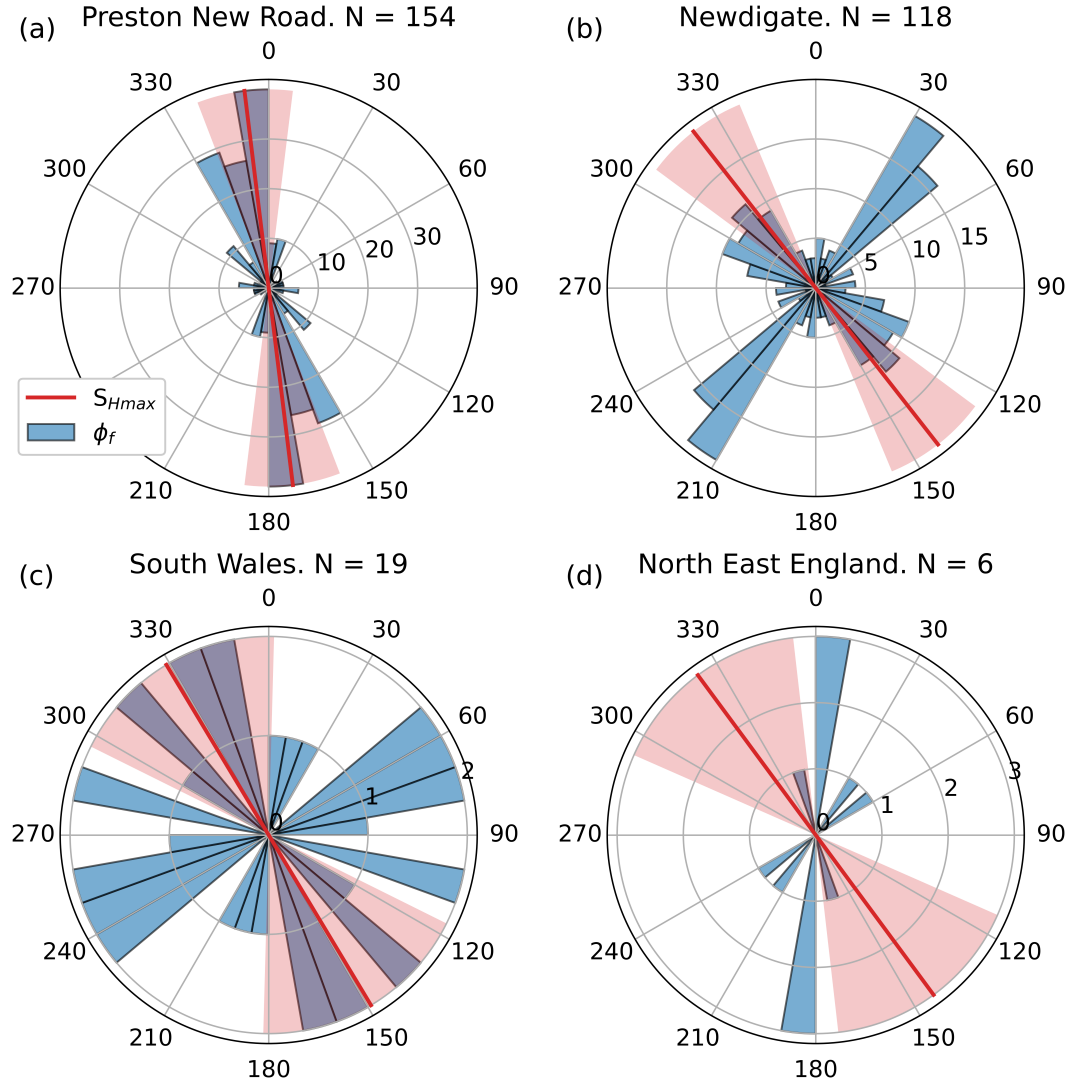
Preston New Road

We make 154 quality A, B, and C shear-wave splitting measurements using data recorded by the Preston New Road surface broadband monitoring stations (Figure 9a). Shear-wave splitting measurements made across the Preston New Road site show a largely unimodal distribution of ϕ_f with a circular mean $\bar{\phi}_f = -16 \pm 27°$. Closer inspection of these results shows a small secondary grouping of 21 measurements which are ca. $90°$ rotated from the mean ϕ_f orientation (Figure 10, 11). Removing measurements with $-70° \leq \phi_f \leq 55°$ results in the circular mean $\bar{\phi}_f = -14 \pm 16°$. Plotting the shear-wave splitting results against earthquake depth shows that there is no correlation between either ϕ_f or δt and depth (Figure 11). To account for variation in δt with ray path length, δt is converted to percentage anisotropy, ξ, following Equation 1 assuming $V_S = 2\,\mathrm{km\,s^{-1}}$.

The Preston New Road results can also be divided by the associated stage of well stimulation. During the stimulation of well PNR-1z, 101 shear-wave splitting measurements are made, and 53 are made for events occurring during the stimulation of PNR-2 in August 2019 (Figure 10). There is little variation in $\bar{\phi}_f$ or ξ between the two stages. With the

34

previously described anomalous measurements removed $\bar{\phi}_f = -14 \pm 14°$ during the stimulation of PNR-1z and $\bar{\phi}_f = -16 \pm 19°$ during the stimulation of PNR-2. Of the 21 anomalous measurements, 16 a recorded in data from PNR-1z and 5 in data from PNR-2.

Whilst there is no World Stress Map data close to Preston New Road, there is additional stress data interpreted from analysis of borehole breakout and drilling induced tensile fractures for the nearby Preese Hall well (PH-1). Previous analysis of data from PH-1 gives a regional S_{Hmax} orientation of $173 \pm 7°$ (Figure 9a; Clarke et al., 2019a).

Newdigate, Surrey

We make 118 quality A, B, and C shear-wave splitting measurements for data from the Newdigate swarm (Figure 9b). The shallow focal depths, ranging from $2\,km$ to $3.6\,km$, impose tight shear-wave window constraints. Due to this restriction nearly all of the shear-wave splitting measurements are made at either STAN, a station North of the Newdigate Fault, or RUSH, a station South of the Newdigate Fault (Figure 13). As there is a clear bimodal distribution in ϕ_f a regional $\bar{\phi}_f$ is not taken and instead we calculate $\bar{\phi}_f$ for STAN and RUSH. There are 55 measurements for STAN, which have a circular mean $\bar{\phi}_f = -51 \pm 26°$ and a mean ξ of 1.87% with a standard deviation of 0.80 (Figure 12a). Percent anisotropy, ξ, is calculated following equation 1 assuming $V_S = 1.66\,km\,s^{-1}$ using a 1-D velocity model for the region (Hicks et al., 2019). There are 54 measurements for RUSH, with a mean $\bar{\phi}_f = 40 \pm 20°$ and a mean ξ

Figure 9: Rose histograms of shear-wave splitting fast polarisations, ϕ_f, (blue bars) for Preston New Road (**a**), North East England (**b**), South Wales (**c**) and Newdigate (**d**). See Figure 7b for region extents. S_{Hmax} orientation for each region is shown by the red lines, with the circular standard deviation shown by the shaded region.
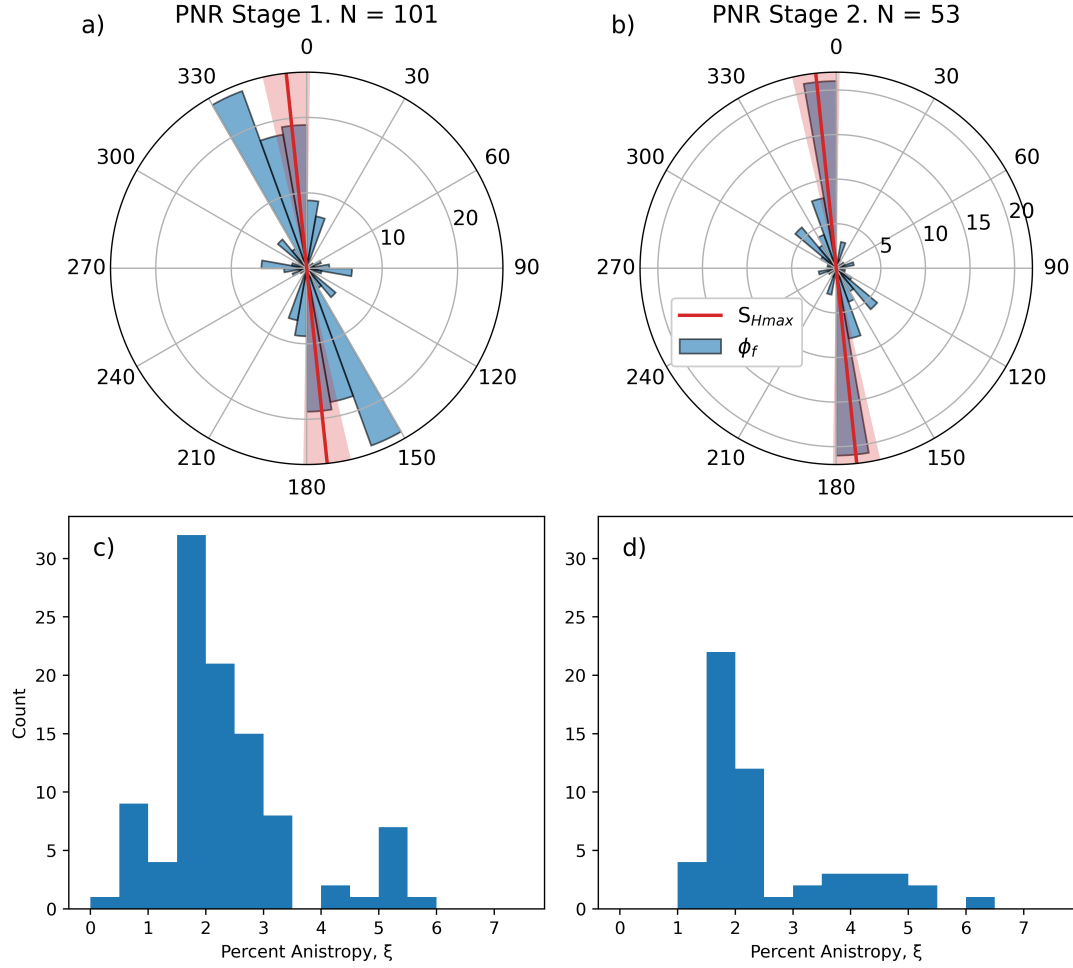
Figure 10: Shear-wave splitting results for Preston New Road split by associated stage of injection. Panels (**a**) and (**b**) show rose histograms of the fast polarisations, ϕ_f, for Stage 1 and Stage 2 respectively and the local S_{Hmax} orientation of $173 \pm 7°$ interpreted from PH-1 (Clarke et al., 2019a). Panels (**c**) and (**d**) show histograms of percentage anisotropy, ξ, calculated following Equation 1 assuming $V_S = 2\,\text{km}\,\text{s}^{-1}$.
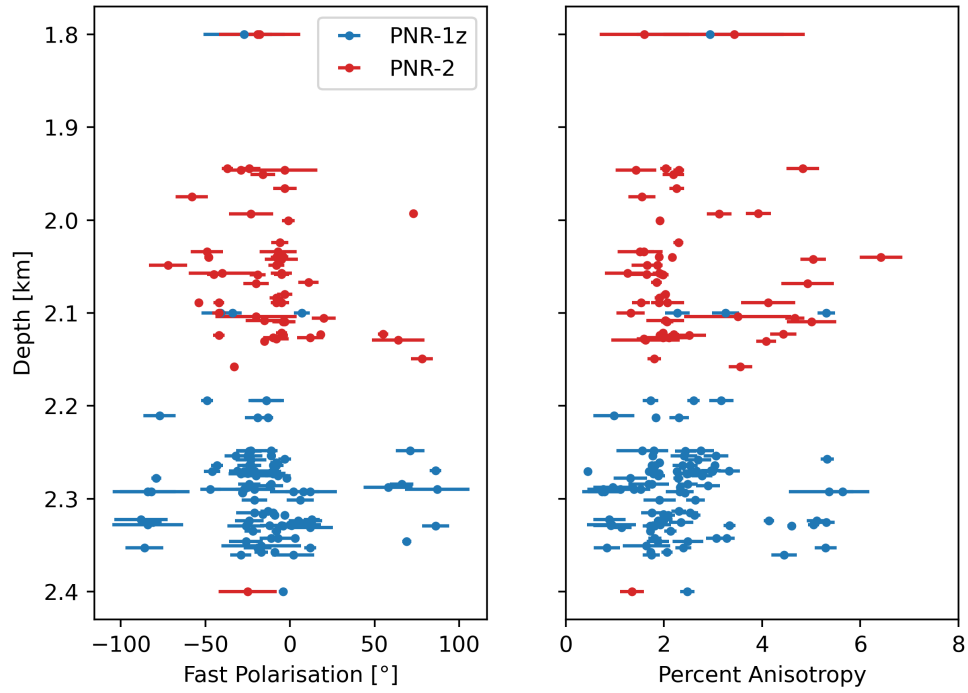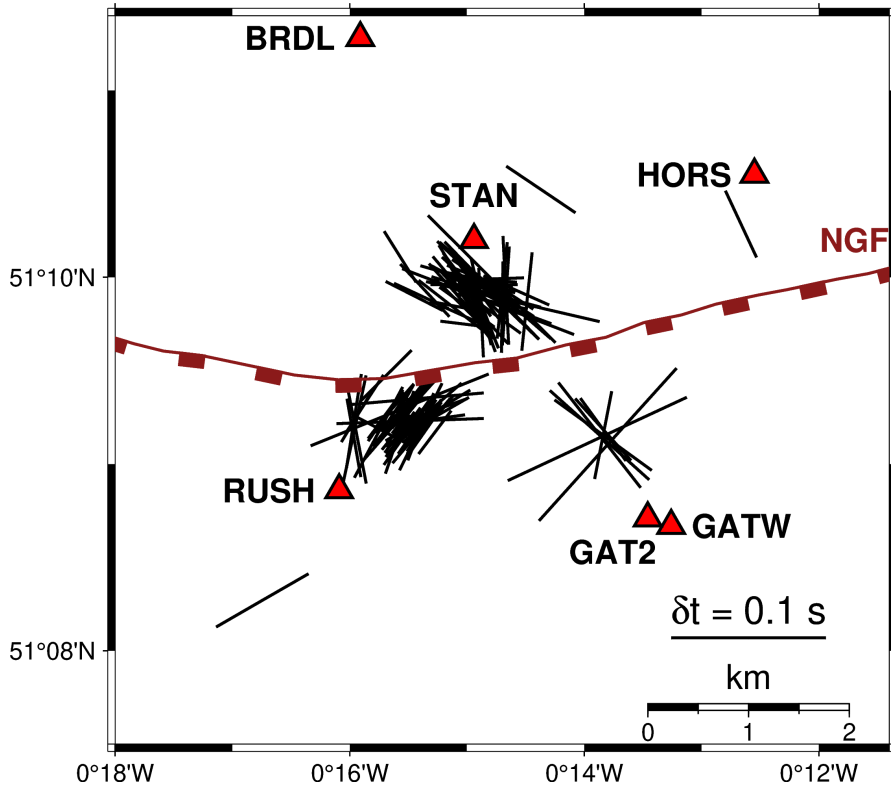
Figure 11: Shear-wave splitting measurements made for microseismicity recorded during the stimulation of PNR-1z (blue) and PNR-2 (red) plotted as a function of earthquake depth. Left panel shows ϕ_f and right panel shows percentage anisotropy, ξ, calculated following Equation 1 assuming $V_S = 2\,\mathrm{km\,s^{-1}}$.
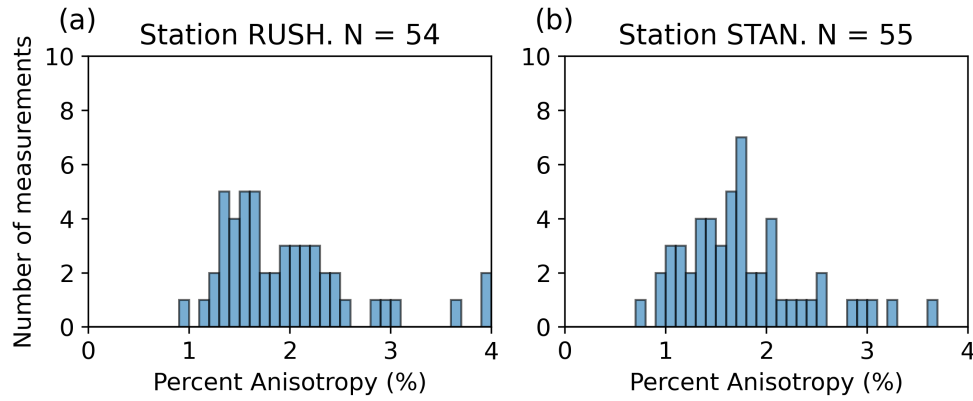
Figure 12: Histograms showing the percent anisotropy, ξ, calculated from δt for each measurement of shear-wave splitting at stations STAN (**a**) and RUSH (**b**). We calculate ξ following equation 1 assuming $V_S = 1.66\,\mathrm{km\,s^{-1}}$ using a 1-D velocity model for the region (Hicks et al., 2019)

.

of 2.16 with a standard deviation of 0.99 (Figure 12b). The remaining measurements are made at GAT2 (6), GATW (1), and HORS (1). No measurements are made for BRDL.

In total 20 breakout zones were interpreted for six boreholes across the Weald with a combined length of over $350\,\mathrm{m}$ (Fellgett and Williams, 2025). Two of the S_{Hmax} interpretations are quality C and four are quality D following the World Stress Map criteria (Heidbach et al., 2016). When taken together, the dominant orientation of the maximum horizontal stress is $142°$ across the six boreholes, with a circular standard deviation of $15°$. This trend is in line with the expected regional orientation of S_{Hmax} in the

Figure 13: Map of shear-wave splitting measurements for Newdigate, Surrey. Measurements are plotted as bars oriented from North by ϕ_f at the midpoint of an assumed linear ray path from source to receiver. The length of the bar is proportional to the measured delay times.

UK (Kingdon et al., 2016) which has previously been attributed to ridge push in the North Atlantic (Klein and Barr, 1986).

South Wales

In South Wales we make 19 measurements of shear-wave splitting for earthquakes with depths in the range $10\,\text{km} - 25.6\,\text{km}$ and local magnitudes in the range $0.5 \leq \text{M}_\text{L} \leq 2.7$. Here the distribution of fast polarisation measurements are bimodal (Figure 9c). Figure 15 shows the splitting measurements plotted halfway along the shear-wave raypath, an approximation which reflect that splitting accumulates between the source
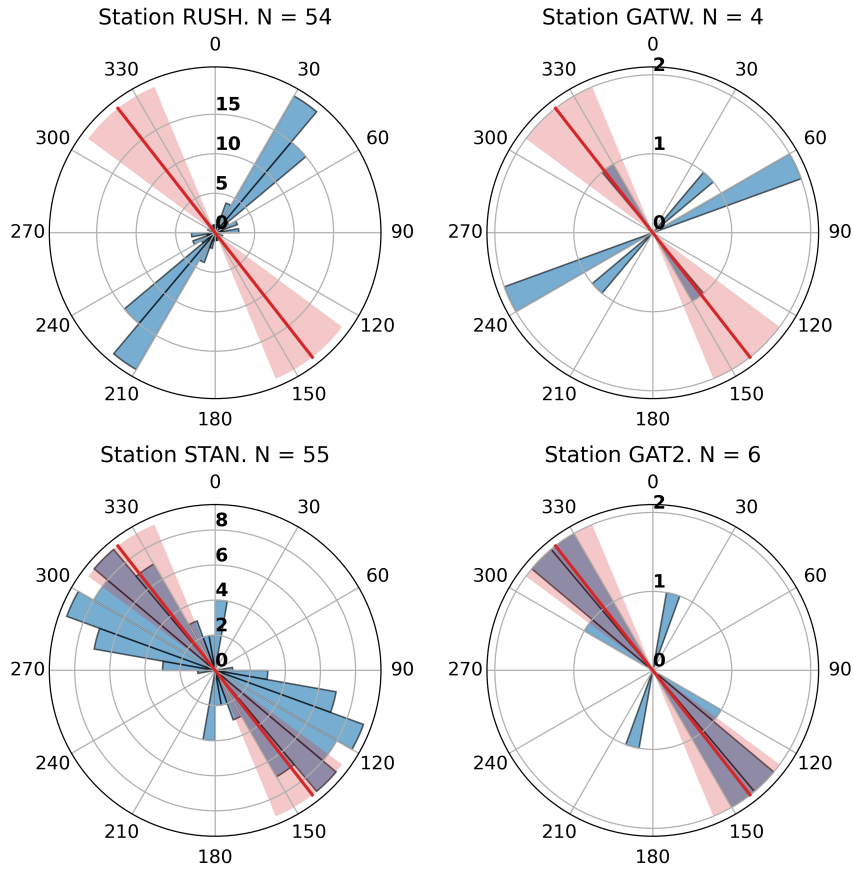
Figure 14: Rose histograms of fast polarisation directions measured at 4 stations (RUSH, STAN, GATW and GAT2) at Newdigate, Surrey. Red bar shows the mean regional S_{Hmax} interpreted for the Weald of $142°$ with a circular standard deviation of $15°$.
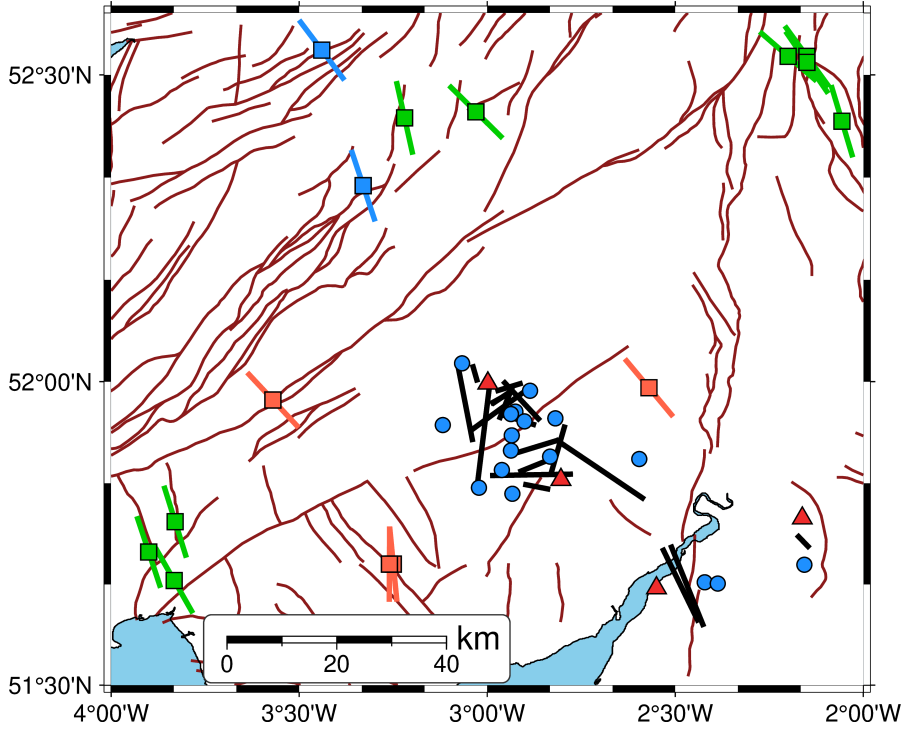
Figure 15: Map showing shear-wave splitting results for South Wales and stress data taken from the Stress Map of Great Britain and Ireland (Kingdon et al., 2022). Shear-wave splitting measurements are plotted as bars located at the earthquake-station midpoint where the bar orientation shows the measured fast polarisation direction and bar length is proportional to δt. Stress data is plotted following Figure 7a. Faults longer than $10\,\mathrm{km}$ in the British Geological Survey 625k database (Survey, 2021) shown by brown lines.

and receiver, and data from the Stress map of Great Britain and Ireland 2022 (Kingdon et al., 2022). The stress data across South Wales has a circular mean of $145°$ and a circular standard deviation of $33°$. Given the small number of measurements and the apparent bimodality of ϕ_f we do not compute summary statistics for the shear-wave splitting results. Plotting ϕ_f and ξ, which is calculated from δt using equation 1 assuming $V_S = 3\,\mathrm{km\,s^{-1}}$, against earthquake depth (Figure 16) shows that $\phi_f, \delta t$ do not vary with depth.
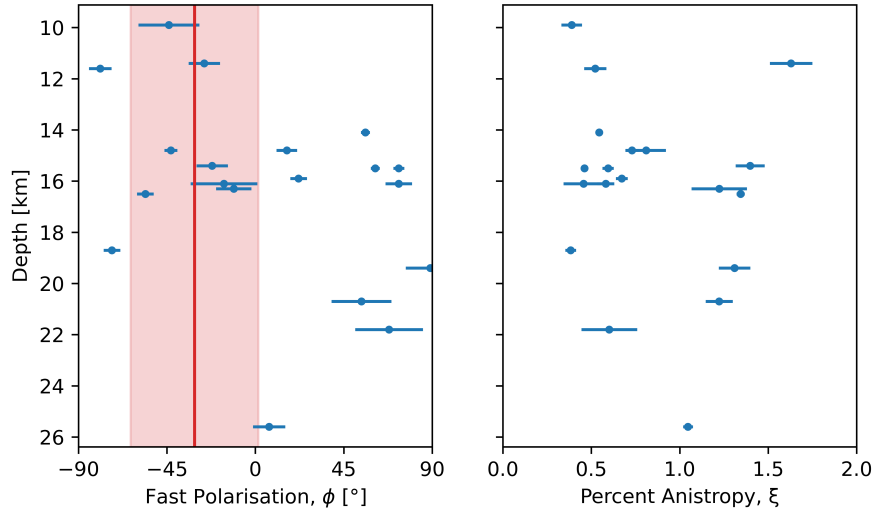
Figure 16: Shear-wave splitting measured for South Wales as a function of depth. Shear-wave splitting delay times, δt are converted to % anisotropy, ξ, following equation 1 assuming a mean V_S of $3\,\mathrm{km\,s^{-1}}$. Red bar shows the circular mean $\mathrm{S_{Hmax}}$ orientation of $149°$ South Wales with the shaded region representing the circular standard deviation $33°$.

Northeast England

There are six measurements of shear-wave splitting in this region which are quality A, B, or C, measured for earthquakes with depths ranging from $9.6\,\mathrm{km}$ to $31.4\,\mathrm{km}$ and local magnitudes in the range $1.2 \leq \mathrm{M_L} \leq 2.6$. The circular mean of the 14 $\mathrm{S_{Hmax}}$ azimuth data points from the Stress Map of Great Britain and Ireland (Kingdon et al., 2022) in the region is $144°$ with a circular standard deviation of $30°$, which is consistent with the NW-SE $\mathrm{S_{Hmax}}$ orientation predominately seen across the UK.

43
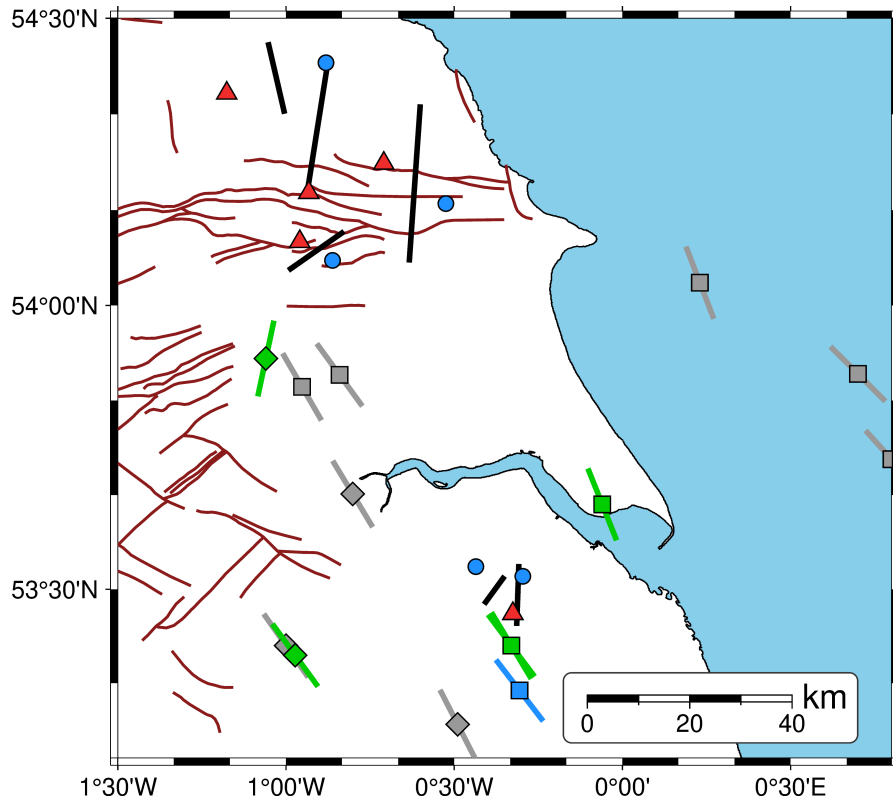
Figure 17: Map showing shear-wave splitting results for North East England and stress data taken from the Stress Map of Great Britain and Ireland (Kingdon et al., 2022). Shear-wave splitting measurements are plotted as bars located at the earthquake-station midpoint where the bar orientation shows the measured fast polarisation direction and bar length is proportional to δt. Faults longer than $10\,\mathrm{km}$ in the British Geological Survey 625k database (Survey, 2021) shown by brown lines. Stress data are plotted following Figure 7a.

Discussion

Seismic anisotropy, measured using shear-wave splitting, can be used to passively measure *in situ* S_{Hmax} azimuth in the upper crust. Here we have linked shear-wave splitting measurements to borehole measurements of stress using onshore UK data. This provides an important reference point of expected S_{Hmax}, which provides important context for the interpretations of the shear-wave splitting results. The four case studies shown here highlight the potential for shear-wave splitting to monitor *in situ* S_{Hmax} azimuth and, and also the challenges to both making measurements and interpreting shear-wave splitting results.

Preston New Road

Shear-wave splitting fast polarisation directions aggregated across the entire Preston New Road dataset show good agreement between ϕ_f and the interpreted S_{Hmax} (Figure 9a). As there is no evidence of depth varying anisotropy, it is clear we are sampling anisotropy in the formations overlying the formation target for hydraulic fracturing, the Bowland Shale. This is largely to be expected, given that the majority of the seismicity occurs within the Bowland Shale and shear-wave splitting accumulated along the entire shear-wave raypath. Therefore we interpret that the shear-wave splitting is sampling stress-induced anisotropy in the overlying formations, with a S_{Hmax} azimuth of $-14 \pm 16°$. For the Preston New Road data, we can also break shear-wave splitting data up by hydraulic fracture stage (Figure 10). In this case this shows that the overall S_{Hmax} parallel

45

trend in ϕ_f is consistent between the two stages of hydraulic fracturing and there is little evidence of a significant temporal variation in shear-wave splitting, and therefore stress and fracture properties, in the overburden between the two stages of injection at Preston New Road.

Newdigate

Newdigate shows a more complicated pattern in shear-wave splitting, particularly in ϕ_f. Results at STAN show a good agreement between ϕ_f and S_{Hmax}, whilst the results and RUSH show a consistent ϕ_f which discrepant by approximately $90°$ (Figure 13, 14). There are several possible explanations for the $90°$ discrepancy between the ϕ_f measured at these two stations (Figure 9b, 14). The most simple, given the temporary nature of the deployment, is sensor misalignment at RUSH, where the horizontal components have been incorrectly aligned. Inspecting waveforms for a teleseismic S arrival recorded by both stations show very strong agreement between the North and East component waveforms which shows that the horizontal components at both stations have the same alignment (Figure 18).

Another possible explanation is structural anisotropy due to the Newdigate fault zone. There are several problems with this explanation. Firstly, the Newdigate fault is small relative to faults where structural anisotropy has been observed (e.g., Boness and Zoback, 2006; Jiang et al., 2021; Okada et al., 2024). Secondly, plotting the shear-wave splitting results at the ray midpoint, which approximates the location of anisotropy, shows the ϕ_f

46
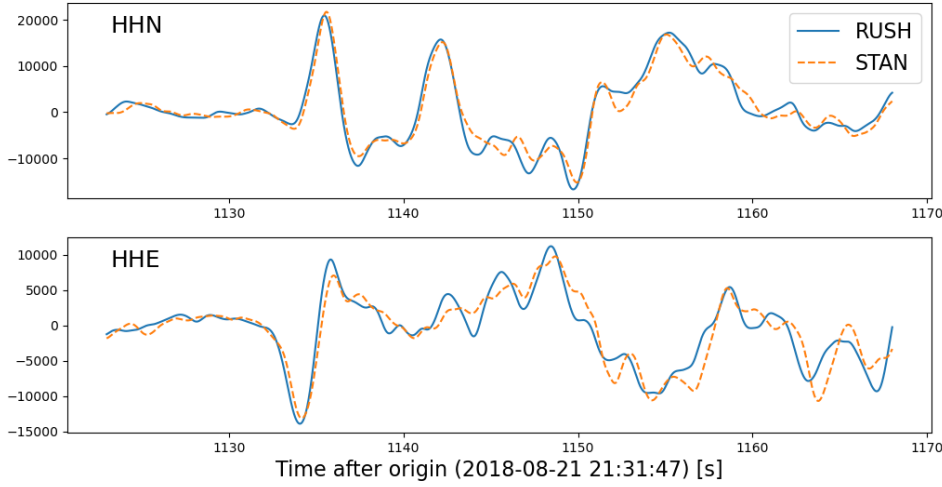
Figure 18: Teleseismic S arrival recorded at stations RUSH (blue, solid line) and STAN (orange, dashed line) during the 2018-9 Newdigate sequence. Note the similarity of the waveforms for the main S arrival. This demonstrates that both sensors were correctly oriented during the Newdigate sequence.

measured at STAN primarily samples the Northern side of the Newdigate fault, whilst measurements at RUSH sample the Southern side. We would expect to see the same structural anisotropy on both sides of the fault, not a $90°$ discrepancy in ϕ_f. Finally, we would expect the microcracks, and therefore ϕ_f, associated with structural anisotropy with to be aligned with E-W strike of the Newdigate fault. The results at both STAN and RUSH do not show this and therefore structure controlled anisotropy from our interpretation.

Given that the ϕ_f data at STAN suggests stress-induced anisotropy to the North of the Newdigate fault, another interpretation could be that these initially contradictory ϕ_f measurements in fact represent a $90°$ rotation in S_{Hmax}. Similar interpretations have been made for observations of $90°$ variations in ϕ_f in volcanic settings where significant changes in S_{Hmax} can

47

be expected during dike injection (e.g., Gerst and Savage, 2004). However such observations in volcanic settings have been for temporal variations in S_{Hmax} rather than sharp spatial variations. Furthermore, the ϕ_f data at GAT2, which is also South of the Newdigate Fault (Figure 13), shows good agreement with S_{Hmax} which would support a consistent regional S_{Hmax} North and South of the Newdigate Fault. Ideally there would be independent *in situ* measurements of S_{Hmax} North and South of the Newdigate fault to confirm it is constants. However it seems implausible that there is a $90°$ rotation in the stress state between the northern and southern fault blocks.

A more plausible interpretation stems from the anisotropic poroelasticity model (APE), which describes stress-induced anisotropy (Zatsepin and Crampin, 1997; Crampin and Zatsepin, 1997). In the case where pore fluids are significantly overpressured $90°$ 'flips' in ϕ_f are predicted (Zatsepin and Crampin, 1997). This behaviour has been previously interpreted for reservoir-scale data (Liu et al., 1997; Angerer et al., 2002; Teanby et al., 2004a) and active fault zones (Liu et al., 1997; Crampin et al., 2002), although the shear-wave splitting observed by Liu et al. (1997) could be plausibly attributed to structural anisotropy due to the San Andreas Fault. At the Valhall reservoir, a useful analogue for offshore CO_2 storage, Teanby et al. (2004a) observed a consistent distribution of $90°$ discrepancies similar to what is seen for Newdigate. One key difference is timescale. The shear-wave splitting measurements at Valhall were for two months (June and July 1997; Teanby et al., 2004a) whilst for Newdigate the $90°$ discrepancy is observed for the entirety of the Newdigate sequence,

at stations STAN and RUSH, from June 2018 until July 2019. However, for the two closely located Gatwick stations GATW and GAT2 we do observe a temporal $90°$ flip in ϕ_f. The ϕ_f measured for GATW, deployed from August 2018 to May 2019, is $90°$ flipped from S_{Hmax} whilst the ϕ_f measured at GAT2, deployed in June 2019, agrees with the regional S_{Hmax} orientation (Figure 13, 14). This temporal change in ϕ_f suggests that there were overpressured pore fluids to the South East of the Newdigate earthquake sequence, causing the $90°$ flip in ϕ_f, and the pressure dropped sufficiently in May 2019 for APE to revert to ϕ_f being aligned with regional S_{Hmax}. Typically such a polarisation flip would also be associated with a decrease in ξ, however the ξ measured at STAN and RUSH is consistent. The $90°$ polarisation flip at RUSH is also consistent throughout the sequence. This would suggest that, if the change in splitting is due to overpressured pore fluids there has not been a drop in pore fluid pressure during earthquake swarm for its entire duration.

As the Weald Basin is exceptionally seismically quiet, and the seismic stations were only deployed to monitor the Newdigate sequence, there is no shear-wave splitting data available before or after the sequence to provide a measure of the background stress field. The nature of the source and receiver geometry also means that RUSH, STAN, GATW, and GAT2 sample a limited azimuthal range, which makes it challenging to completely rule out more complicated anisotropic fabrics. It could be possible that there cross-cutting microcracks, with the set oriented perpendicular to S_{Hmax} being cemented. However, microcracks filled with a solid are significantly less effective at producing seismic anisotropy

(Hudson, 1981; Crampin, 1999) and there is no clear difference in δt between RUSH and STAN (Figure 13).

The most plausible interpretation is APE on both sides of the Newdigate Fault, with the $90°$ discrepancies in ϕ_f caused by overpressured pore fluids to the South of the Newdigate Fault. This does, however, raise further questions which should be investigated. How significant must the overpressure be to produce the ϕ_f flips observed and is this plausible? Is it hydrogeologically feasible to maintain these pressures persist throughout, and likely before and after, the Newdigate sequence in at least part of the Southern fault block? More detailed analysis, implementation of the APE model and studying any available regional pore fluid pressure data is required to further interrogate the $90°$ discrepancy in ϕ_f at Newidgate. If additional monitoring stations could have been deployed during the Newdigate sequence, particularly to the South of the Newdigate fault, the additional data at a different azimuths would significantly improve our ability to test this hypothesis.

South Wales

For South Wales, there is a clear bimodal distribution in the shear-wave splitting results. Whilst one population of ϕ_f does agree with the estimated region S_{Hmax}, there are a similar number of measurements which do not (Figure 9c). Figure 15 shows that all the data points which do not align with S_{Hmax} are located between the two stations in South Wales. As with Newdigate, the two populations of ϕ_f are sub-perpendicular and the shear-

50

wave splitting measurements surround the Neath Disturbance, a major fault structure in South Wales which is expected to be a significant structure at depth (Blenkinsop et al., 1986; Survey, 2021). However, unlike Newdigate the ca. $90°$ rotation is seen for measurements at the stations on both sides of the fault.

One explanation could be multiple layers of anisotropy, but the splitting results show no evidence for depth varying splitting. This suggests the anisotropy accumulated in the upper $10\,\mathrm{km}$ of the crust. The lack of depth dependence also makes multiple anisotropic layers unlikely, but the South Wales data has insufficient azimuthal coverage to fully test this hypothesis. An alternate hypothesis is structural controlled anisotropy from the Neath Disturbance. Significant fault structures are well known to produce structural controlled anisotropy in their vicinity, producing an anisotropic fabric where the shear-wave splitting fast polarisation direction is aligned with fault strike (e.g., Boness and Zoback, 2006; Jiang et al., 2021; Okada et al., 2024). In this case the measured ϕ_f which do not align with S_{Hmax} do align well with the the strike of the Neath Disturbance. This suggests that in the vicinity of the fault, we are observing structure controlled anisotropy.

Northeast England

The lack of shear-wave splitting data, with only six data points, in this region makes any interpretation challenging. However, the measured ϕ_f largely do not agree with the regional mean S_{Hmax} (Figure 9d). The

51

sparse data makes is difficult to interrogate why the splitting deviates from S_{Hmax}. However, the shear-wave splitting also does not not align with regional fault structures (Figure 17), which are predominantly East-West trending, which suggested there is no structural component to the anisotropy. With no obvious structural controlled anisotropy, it is possible that this discrepancy is indicative local scale variations in S_{Hmax} which has been observed elsewhere in the UK (Hudson et al., 2024a).

The future of shear-wave splitting for stress field monitoring

The advantages of shear-wave splitting is that it is a passive measurement and, as such, a few well positioned stations that make a few high quality measurements have the potential to add important constraints on the *in situ* stress field at a spatial resolution which cannot be achieved by borehole measurements. Earthquake focal mechanisms also can be used to characterise the stress field, but require many observations over a wide range of azimuths which can be difficult to achieve for microseismicity.

Preston New Road serves as a good analogue for potential industrial applications, such as CO_2 injection, geothermal plants, hydraulic fracturing, and geological disposal facilities. This case study shows that when a site is well instrumented, shear-wave splitting can be used as an independent measure of S_{Hmax} azimuth. In this case the measured ϕ_f are consistent with S_{Hmax} interpreted from the nearby PH-1 well, with the shear-wave splitting providing and additional independent datapoint that validates the previously interpreted S_{Hmax} azimuth at Preston New Road.

This ability of shear-wave splitting to act as an independent measure of S_{Hmax} is particularly important for industrial subsurface projects as it can detect local scale spatial deviations in the stress field, which has been observed in Cornwall (Hudson et al., 2024a).

One advantage of using shear-wave splitting for monitoring the *in situ* stress field is that temporal variations in shear-wave splitting can be used to resolved changes stress. Time varying signatures in ϕ_f have been associated with stress changes due to crustal processes (e.g., Crampin et al., 1999; Liu et al., 2014) and during dike injection at depth (e.g., Gerst and Savage, 2004; Johnson et al., 2011) or heating of hydrothermal systems (Kendall et al., 2025) prior to volcanic eruptions. Temporal variation in δt or ξ is associated with a change in fracture properties such as fracture density, length, or aspect ratio, which can be stress-induced (Kendall et al., 2025). At Preston New Road no evidence of temporal variation in shear-wave splitting was observed, the ideal null result for stress monitoring of storage integrity as it suggests no change in the stress field in the overburden formations. Temporal variations in shear-wave splitting can also occur in response to changes in pore fluid pressure, as seen at Newdigate. For onshore and offshore project where microseismic monitoring is common practice or a regulatory requirement, the ability for shear-wave splitting to passively sample the *in situ* stress field and potentially to constrain fracture properties and pore fluid pressures adds significant value to monitoring networks.

The sensitivity to temporal variations means that S_{Hmax} azimuths from shear wave splitting need to be ground truthed against more traditional

methods such as borehole breakouts analysis. However, borehole breakouts usually only allow for static interpretations of S_{Hmax} azimuth at the time of drilling. Once drilling is completed most boreholes are sealed or screened so it is not possible to reacquire data to investigate time dependent variations in S_{Hmax} azimuth. If data can't be required from the same borehole the only other way to assess temporal variations is to drill into the same formation from a nearby location. However, drilling boreholes is expensive and examples of drilling multiple boreholes across many years are rare.

Localised temporal shifts in S_{Hmax} azimuth can be observed from interpreted borehole breakouts. Following the magnitude 6.9 earthquake near Kobe in 1995 there was a significant localised shift in breakout orientations. When the same strata were drilled again in 2017 breakout orientations had shifted to the regional stress field orientation (Nishiwaki et al., 2018).

In addition, methods to improve confidence S_{Hmax} azimuths from breakout orientations will remove any localised depth or stratigraphic variations in S_{Hmax} azimuth. Furthermore, in the UK and UKCS many boreholes used in interpretation of S_{Hmax} azimuth are drilled by the hydrocarbon industry so are heavily biased to economic strata.

As a result, where variations in S_{Hmax} azimuths are observed from breakouts it is difficult to interpret whether it is the result of an isolated localised variation. For example, in the Back Lane Plugnar borehole in the UK there are four S_{Hmax} azimuths recorded from hydraulic fracturing

54

(Cooling et al., 1988). Three of the observations are from Triassic and Carboniferous sediments which show similar S$_{\text{Hmax}}$ azimuths (140–155°), with a single observation at $90\,\text{degree}$ to it from carboniferous volcanics. As volcanics are under-represented in borehole drilled in Great Britain it not possible to conclude whether this is a localised variation of whether stress field rotations are more likely in volcanics. As a catalogue of shear wave splitting measurements are created they will create more opportunities to categorise the variations in the stress field orientation in space and time which are beyond the current methodologies.

There are, however, challenges with using shear-wave splitting to monitor *in situ* stress. As shear-wave splitting is a passive measurement, it is dependent on microseismicity occurring within the shear-wave window of monitoring stations. This likely requires either significant microseismicity or dense local monitoring networks. To integrate shear-wave splitting into a monitoring program the deployment of the microseismic network should include stations where the distance from the station to any potential sources of microseismicity (i.e., a mapped fault or the injector wells) is less than the reservoir depth.

For industrial applications, the instrumentation challenge can be overcome. The shear-wave window challenge can be overcome by deploying denser, targeted monitoring networks, which are becoming more feasible with instrumentation advances. For onshore monitoring instrumentation advances may make this feasible at reasonably low cost, with seismic nodes being shown to have good potential to measure shear-wave splitting when arranged to form an effective 3-component instrument (Hudson et al.,

2024a) and three-component broadband nodes have also been developed.

Ocean bottom nodes or permanent reservoir monitoring systems may be feasible to achieve similar results for offshore projects. However, there have thus far been no studies exploring the potential of these sea floor systems. As shear-wave splitting measurements from microseismicity are sensitive to noise levels, future work studying data recorded by existing seafloor monitoring systems is needed to ensure measurements can be made in this setting.

A second challenge is that in some localities the seismic anisotropy can be heterogeneous and before we can use shear-wave splitting as a proxy for stress we must be confident that stress-induced anisotropy is the predominant mechanism. In many settings it can be difficult to distinguish between structural and stress-controlled seismic anisotropy (e.g., Pastori et al., 2019). This interpretation challenge is highlighted by the results for South Wales and Newdigate. In South Wales, additional geological context makes it clear that what may appear as significant local deviations in S_{Hmax} are in fact most likely a change in mechanism from stress-induced anisotropy to structural (fault controlled) anisotropy. At Newdigate, despite the wealth of seismicity data, it is still challenging to definitively explain the mechanism responsible for the $90°$ flip in ϕ_f North and South of the Newdigate Fault. Our preferred interpretation is that overpressured pore fluids in the Southern fault block. This, however, does lead to the conclusion that pore fluids remain overpressured throughout the Newdigate sequence and the hypothesis requires further interrogation.

For industrial applications, the additional contextualising geological and geophysical data collected when characterising the subsurface for a project will simplify the interpretation. With better data on porefluid pressure, fault locations and subsurface geology some of the interpretation challenges encountered here, such as for Newdigate and South Wales, can be more easily resolved.

For well instrumented regions, where the baseline seismic velocities and anisotropy of a region are well characterised then the potential of shear-wave splitting can be pushed further. For dense datasets, it is possible to constrain subsurface fracture properties by using frequency-dependent shear-wave splitting (Al-Harrasi et al., 2011) or by inverting shear-wave splitting measurements (Verdon et al., 2009; Verdon and Kendall, 2011, e.g.,). The delay times for fracture induced shear-wave splitting are dependent on fracture density and aspect ratio, which we know from the APE model are controlled by differential horizontal stress in the case of vertically aligned fractures. A promising area of future research is to combined advances in shear-wave splitting inversion (Wookey, 2012; Kufner et al., 2023; Asplet et al., 2023), with existing fracture inversion methods and the APE model to invert shear-wave splitting delay times for differential horizontal stress. An ideal experiment would be for a well-understood reservoir where existing geomechanical models could be used to calibrate the results.

Conclusion

We have shown how shear-wave splitting of shallow microseismicity can be used to monitor *in situ* stress. Additional means of constraining stress or fracturing for various subsurface geological storage, or geofluid extraction, are highly valuable. For geological CO_2 storage, monitoring the *in situ* stress in the storage complex prior to, during, and after injection can be used to calibrate geomechanical models of the reservoir and to ensure long-term storage integrity. By studying different settings across the UK, we highlight the potential of shear-wave splitting as a passive measure of *in situ* stress, and also the challenges that remain, particularly that of the shear wave window and ensuring interpretations of stress-induced seismic anisotropy are robust. We find that:

1. At Preston New Road, Lancashire, the best direct analogue for CO_2 injection in the UK dataset, we measure shear-wave splitting due to stress-induced seismic anisotropy and interpret a S_{Hmax} azimuth consistent with nearby borehole breakout data.

2. At Newdigate, Surrey, we observe shear-wave splitting which is best explain by stress induced anisotropy, which is consistent with regional S_{Hmax} except where there are polarisation flips likely due to overpressured pore fluids.

3. In South Wales, we observe structural and stress controlled seismic anisotropy. Measurements close to the Neath Disturbance show ϕ_f parallel to the strike of this major fault. For measurements further

58

away form the fault, ϕ_f returns to being parallel to S_{Hmax}, consistent with stress-controlled seismic anisotropy.

Given that shear-wave splitting could enable passive, semi-continuous, measurements of the stress field in the caprock and overburden units, its potential should be explored further. Future research to improve existing shear-wave splitting inversion methods to incorporate existing rock physics models and other seismic constraints of stress such as focal mechanisms, could allow for the shear-wave splitting to be inverted for S_{Hmax} azimuth and differential horizontal stress. If this link can be formalised, shear-wave splitting has the potential to become a key tool for monitoring *in situ* stress for subsurface geological storage, geothermal, and hydrocarbon projects.

In the case of offshore CO_2 storage projects, where offshore microseismic monitoring infrastructure is desirable, incorporating shear-wave splitting into the design of monitoring networks will enable highly valuable additional datasets to be collected. Further studies, using data from existing seafloor instrumentation, such as permanent reservoir monitoring systems, is required to assess the suitability of shear-wave splitting in offshore settings.

Acknowledgements

Funding Information

Author Contributions

JA: conceptualization (equal), data curation (lead), formal analysis (lead), investigation (lead), methodology (lead), visualisation (lead), writing – original draft (lead), writing – review and editing (lead). MF: formal analysis (supporting), investigation (supporting), writing - original draft (supporting), writing - review and editing (supporting). TK: conceptualization (equal), data curation (supporting), writing – review and editing (supporting). JMK: conceptualization (equal), funding acquisition (lead), writing – review and editing (supporting).

Data Availability

This publication is supported by multiple datasets, which are openly available at locations cited in the data section. Stress data is available from the World Stress Map (Heidbach et al., 2018) and the British Geological Survey (Fellgett and Williams, 2025). Earthquake data are available from the British Geological Survey Seismicity Catalogue (British Geological Survey, 2025). Additional earthquake data for Newdigate is taken from Hicks et al. (2019) and for Preston New Road is taken from Clarke et al. (2019b) and Kettlety et al. (2020). Waveform data is taken from the BGS EIDA node for network codes GB (British Geological Survey, 1970) and UR (British Geological Survey, 2015). Shear-wave splitting results are available in the Zenodo repository 10.5281/zenodo.17048208. Data from the Open Street Map (OpenStreetMap contributors, 2017) and the

British Geological Survey 625k fault dataset (Survey, 2021) is used in some figures.

Competing Interests

The authors declare that they have no known competing financial interests or personal relationships that could have appeared to influence the work reported in this paper.

References

Abt, David L. and Karen M. Fischer (2008). "Resolving three-dimensional anisotropic structure with shear wave splitting tomography". In: *Geophysical Journal International* 173.3, pp. 859–886. ISSN: 1365246X. DOI: `https://doi.org/1 0.1111/j.1365-246X.2008.03757.x`.

Angerer, Erika, Stuart Crampin, Xiang-Yang Li, and Thomas L. Davis (May 2002). "Processing, modelling and predicting time-lapse effects of overpressured fluid-injection in a fractured reservoir". In: *Geophysical Journal International* 149.2, pp. 267–280. ISSN: 0956-540X. DOI: `https://doi.org/10.1046/j.1365-246 X.2002.01607.x`.

Asplet, Joseph, James Wookey, and Michael Kendall (2020). "A potential post-perovskite province in D″ beneath the Eastern Pacific: evidence from new analysis of discrepant SKS–SKKS shear-wave splitting". In: *Geophysical Journal International* 221.3, pp. 2075–2090. ISSN: 0956-540X. DOI: `https://doi.org/10.1093/gji/ggaa11 4`.

Asplet, Joseph, James Wookey, and Michael Kendall (2023). "Inversion of shear wave waveforms reveal deformation in the lowermost mantle". In: *Geophysical Journal International* 232.1, pp. 97–114. DOI: `10.1093/gji/ggac328`.

Asplet, Joseph, James Wookey, Micheal Kendall, Mark Chapman, and Ritima Das (May 2024). "Shear-wave attenuation anisotropy: a new constraint on mantle melt near the Main Ethiopian Rift". In: *Seismica* 3.1. Section: Articles. DOI: `https://doi.org/1 0.26443/seismica.v3i1.1098`.

Audet, Pascal and Andrew J. Schaeffer (Dec. 2019). *SplitPy: Software for teleseismic shear-wave splitting analysis*. DOI: `https://doi.org/10.5281/zenodo.356478 0`.

Backus, George E. (1962). "Long-wave elastic anisotropy produced by horizontal layering". In: *Journal of Geophysical Research* 67.11, pp. 4427–4440. ISSN: 0148-0227. DOI: `https://doi.org/10.1029/jz067i011p04427`.

Baird, Alan F., J.-Michael Kendall, R. Stephen J. Sparks, and Brian Baptie (2015). "Transtensional deformation of Montserrat revealed by shear wave splitting". In:

Earth and Planetary Science Letters 425, pp. 179–186. ISSN: 0012-821X. DOI: https://doi.org/10.1016/j.epsl.2015.06.006.

Baird, Alan F., J.-Michael Kendall, James P. Verdon, Andreas Wuestefeld, Todd E. Noble, Yongyi Li, Martin Dutko, and Quentin J. Fisher (2013). "Monitoring increases in fracture connectivity during hydraulic stimulations from temporal variations in shear wave splitting polarization". In: *Geophysical Journal International* 195.2, pp. 1120–1131. ISSN: 0956-540X. DOI: https://doi.org/10.1093/gji/ggt274.

Baptie, B. (2021). *Earthquake Seismology 2020/2021 Open Report*. Tech. rep. OR/21/033. British Geological Survey.

Bastow, I. D., T. J. Owens, G. Helffrich, and J. H. Knapp (2007). "Spatial and temporal constraints on sources of seismic anisotropy: Evidence from the Scottish highlands". en. In: *Geophysical Research Letters* 34.5. _eprint: https://onlinelibrary.wiley.com/doi/pdf/10.1029/2006GL028911. ISSN: 1944-8007. DOI: https://doi.org/10.1029/2006GL028911.

Bell, J. S. and D. I. Gough (Nov. 1979). "Northeast-southwest compressive stress in Alberta evidence from oil wells". In: *Earth and Planetary Science Letters* 45.2, pp. 475–482. ISSN: 0012-821X. DOI: https://doi.org/10.1016/0012-821X(79)90146-8.

Beyreuther, M., R. Barsch, L. Krischer, T. Megies, Y. Behr, and J. Wassermann (2010). "ObsPy: A Python toolbox for seismology". In: *Seismological Research Letters* 81.3, pp. 530–533. DOI: 10.1785/gssrl.81.3.530.

Bianco, Francesca, Luciano Scarfi, Edoardo Del Pezzo, and Domenico Patanè (Nov. 2006). "Shear wave splitting changes associated with the 2001 volcanic eruption on Mt Etna". In: *Geophysical Journal International* 167.2, pp. 959–967. ISSN: 0956-540X. DOI: https://doi.org/10.1111/j.1365-246X.2006.03152.x.

Blenkinsop, T. G., R. E. Long, N. J. Kusznir, and M. J. Smith (Mar. 1986). "Seismicity and tectonics in Wales". In: *Journal of the Geological Society* 143.2, pp. 327–334. ISSN: 0016-7649. DOI: https://doi.org/10.1144/gsjgs.143.2.0327.

Boness, Naomi L. and Mark D. Zoback (Oct. 2006). "Mapping stress and structurally controlled crustal shear velocity anisotropy in California". In: *Geology* 34.10, pp. 825–828. ISSN: 0091-7613. DOI: https://doi.org/10.1130/G22309.1.

Booth, David C. and Stuart Crampin (Oct. 1, 1985). "Shear-wave polarizations on a curved wavefront at an isotropic free surface". In: *Geophysical Journal International* 83.1, pp. 31–45. ISSN: 0956-540X. DOI: `https://doi.org/10.1111/j.1365-246X.1985.tb05154.x`.

Bowman, J Roger and Masataka Ando (1987). "Shear-wave splitting in the upper-mantle wedge above the Tonga subduction zone". In: *Geophysical Journal of the Royal Astronomical Society* 88 (March), pp. 25–41. DOI: `https://doi.org/10.1111/j.1365-246X.1987.tb01367.x`.

British Geological Survey (1970). *Great Britain Seismograph Network*. DOI: `https://doi.org/10.7914/AV8J-NC83`.

British Geological Survey (2015). *UKArray*. DOI: `https://doi.org/10.7914/SN/UR`.

British Geological Survey (2025). *British Geological Survey Earthquake Database*. `http://quakes.bgs.ac.uk/earthquakes/dataSearch.html`. Accessed: 2025-03-05.

Carter, Andrew J. and J.-Michael Kendall (2006). "Attenuation anisotropy and the relative frequency content of split shear waves". In: *Geophysical Journal International* 165.3, pp. 865–874. ISSN: 1365-246X. DOI: `https://doi.org/10.1111/j.1365-246x.2006.02929.x`.

Castellazzi, Claire, Martha K. Savage, Ernestynne Walsh, and Richard Arnold (May 2015). "Shear wave automatic picking and splitting measurements at Ruapehu volcano, New Zealand". In: *Journal of Geophysical Research: Solid Earth* 120.5, pp. 3363–3384. ISSN: 2169-9313, 2169-9356. DOI: `https://doi.org/10.1002/2014JB011585`.

Chakraborty, Megha, Georg Rümpker, Wei Li, Johannes Faber, Nishtha Srivastava, and Frederik Link (2024). "Feasibility of Deep Learning in Shear Wave Splitting analysis using Synthetic-Data Training and Waveform Deconvolution". In: *Seismica* 3.1. DOI: `10.26443/seismica.v3i1.1124`.

Chapman, M (2003). "Frequency-dependent anisotropy due to meso-scale fractures in the presence of equant porosity". In: *Geophysical Prospecting* 51.5, pp. 369–379. ISSN: 1365-2478. DOI: `https://doi.org/10.1046/j.1365-2478.2003.00384.x`.

Chevrot, Sebastian (2000). "Multichannel analysis of shear wave splitting". In: *Journal of Geophysical Research: Solid Earth* 105.B9, pp. 21579–21590. ISSN: 0148-0227. DOI: https://doi.org/10.1029/2000jb900199.

Clarke, Huw, Hamed Soroush, and Thomas Wood (2019a). "Preston New Road: The Role of Geomechanics in Successful Drilling of the UK's First Horizontal Shale Gas Well". In: *SPE Europec featured at 81st EAGE Conference and Exhibition*, D041S012R008. DOI: https://doi.org/10.2118/195563-ms.

Clarke, Huw, James P Verdon, Tom Kettlety, Alan F Baird, and J-Michael Kendall (2019b). "Real-time imaging, forecasting, and management of human-induced seismicity at Preston New Road, Lancashire, England". In: *Seismological Research Letters* 90.5, pp. 1902–1915. DOI: 10.1785/0220190110.

Cooling, C. M., J. A. Hudson, and L. W. Tunbridge (1988). "In situ rock stresses and their measurement in the U.K.—Part II. Site experiments and stress field interpretation". In: vol. 25. 6, pp. 371–382. DOI: https://doi.org/10.1016/0148-9062(88)90977-1.

Crampin, S (1999). "Calculable fluid–rock interactions". In: *Journal of the Geological Society* 156.3, pp. 501–514. ISSN: 0016-7649. DOI: https://doi.org/10.1144/gsjgs.156.3.0501.

Crampin, Stuart (1987). "Geological and industrial implications of extensive-dilatancy anisotropy". In: *Nature* 328.6130, pp. 491–496. ISSN: 0028-0836. DOI: https://doi.org/10.1038/328491a0.

Crampin, Stuart, Russ Evans, Balamir Üçer, Mark Doyle, J. Peter Davis, Galia V. Yegorkina, and Alistair Miller (Aug. 1980). "Observations of dilatancy-induced polarization anomalies and earthquake prediction". en. In: *Nature* 286.5776, pp. 874–877. ISSN: 0028-0836, 1476-4687. DOI: https://doi.org/10.1038/286874a0.

Crampin, Stuart, Yuan Gao, and Julian Bukits (Aug. 2015). "A review of retrospective stress-forecasts of earthquakes and eruptions". In: *Physics of the Earth and Planetary Interiors* 245, pp. 76–87. ISSN: 0031-9201. DOI: https://doi.org/10.1016/j.pepi.2015.05.008.

Crampin, Stuart, Yuan Gao, and Sheila Peacock (May 2008). "Stress-forecasting (not predicting) earthquakes: A paradigm shift?" In: *Geology* 36.5, pp. 427–430. ISSN: 0091-7613. DOI: https://doi.org/10.1130/G24643A.1.

Crampin, Stuart, Theodora Volti, Sebastien Chastin, Agust Gudmundsson, and Ragnar Stefánsson (Nov. 2002). "Indication of high pore-fluid pressures in a seismically-active fault zone". In: *Geophysical Journal International* 151.2, F1–F5. ISSN: 0956-540X. DOI: https://doi.org/10.1046/j.1365-246X.2002.01830.x.

Crampin, Stuart, Theodora Volti, and Ragnar Stefánsson (1999). "A successfully stress-forecast earthquake". In: *Geophysical Journal International* 138.1, F1–F5. ISSN: 0956-540X. DOI: https://doi.org/10.1046/j.1365-246x.1999.00891.x.

Crampin, Stuart and Sergei V. Zatsepin (1997). "Modelling the compliance of crustal rock—II. Response to temporal changes before earthquakes". In: *Geophysical Journal International* 129.3, pp. 495–506. ISSN: 0956-540X. DOI: https://doi.org/10.1111/j.1365-246x.1997.tb04489.x.

Fellgett, M. W. and J. D. O. Williams (2025). *SHARP UK and UK Continental Shelf stress field observations*. Dataset. DOI: 10.5285/d3454827-1fe5-4a8d-9d9e-1cf5e4c97886.

Gao, Yuan, Jing Wu, Yoshio Fukao, Yutao Shi, and Ailan Zhu (2011). "Shear wave splitting in the crust in North China: stress, faults and tectonic implications". In: *Geophysical Journal International* 187.2. Publisher: Blackwell Publishing Ltd Oxford, UK, pp. 642–654. DOI: https://doi.org/10.1111/j.1365-246X.2011.05200.x.

Gerst, Alexander and Martha K. Savage (2004). "Seismic Anisotropy Beneath Ruapehu Volcano: A Possible Eruption Forecasting Tool". In: *Science* 306.5701, pp. 1543–1547. DOI: https://doi.org/10.1126/science.1103445.

Goertz-Allmann, Bettina P., Nadège Langet, Kamran Iranpour, Daniela Kühn, Alan Baird, Steve Oates, Carrie Rowe, Stephen Harvey, Volker Oye, and Hilde Nakstad (Mar. 2024). "Effective microseismic monitoring of the Quest CCS site, Alberta, Canada". In: *International Journal of Greenhouse Gas Control* 133, p. 104100. ISSN: 1750-5836. DOI: https://doi.org/10.1016/j.ijggc.2024.104100.

Guzman, Veronica, Aibing Li, and Alexandros Savvaidis (Aug. 2022). "Stress Variations in the Delaware Basin from Shear-Wave Splitting Analysis". In: *Seismological Research Letters* 93.6, pp. 3433–3443. ISSN: 0895-0695. DOI: `https://doi.org/10.1785/0220220118`.

Al-Harrasi, O. H., J.-M. Kendall, and M. Chapman (2011). "Fracture characterization using frequency-dependent shear wave anisotropy analysis of microseismic data". In: *Geophysical Journal International* 185.2, pp. 1059–1070. ISSN: 1365-246X. DOI: `https://doi.org/10.1111/j.1365-246x.2011.04997.x`.

Heidbach, O, Andreas Barth, Birgit Müller, John Reinecker, Ove Stephansson, Mark Tingay, and A Zang (2016). "WSM quality ranking scheme, database description and analysis guidelines for stress indicator". In: *World Stress Map Technical Report 16-01*. DOI: `http://doi.org/10.2312/wsm.2016.001`.

Heidbach, Oliver et al. (Oct. 2018). "The World Stress Map database release 2016: Crustal stress pattern across scales". In: *Tectonophysics* 744, pp. 484–498. ISSN: 0040-1951. DOI: `https://doi.org/10.1016/j.tecto.2018.07.007`.

Helffrich, George (1995). "Lithospheric deformation inferred from teleseismic shear wave splitting observations in the United Kingdom". In: *Journal of Geophysical Research: Solid Earth* 100.B9, pp. 18195–18204. ISSN: 0148-0227. DOI: `https://doi.org/10.1029/95jb01572`.

Hicks, Stephen P., James Verdon, Brian Baptie, Richard Luckett, Zoë K. Mildon, and Thomas Gernon (2019). "A Shallow Earthquake Swarm Close to Hydrocarbon Activities: Discriminating between Natural and Induced Causes for the 2018–2019 Surrey, United Kingdom, Earthquake Sequence". In: *Seismological Research Letters* 90.6, pp. 2095–2110. ISSN: 0895-0695. DOI: `https://doi.org/10.1785/0220190125`.

Hudson, J. A. (1981). "Wave speeds and attenuation of elastic waves in material containing cracks". In: *Geophysical Journal of the Royal Astronomical Society* 64.1, pp. 133–150. ISSN: 1365-246X. DOI: `https://doi.org/10.1111/j.1365-246x.1981.tb02662.x`.

Hudson, Thomas Samuel, Joseph Asplet, and Andrew Walker (June 2023). "Automated shear-wave splitting analysis for single- and multi- layer anisotropic media". In: *Seismica*. DOI: https://doi.org/10.31223/x5r67z.

Hudson, Thomas Samuel, Tom Kettlety, John-Michael Kendall, Tom O'Toole, Andrew Jupe, Robin K Shail, and Augusta Grand (2024a). "Seismic Node Arrays for Enhanced Understanding and Monitoring of Geothermal Systems". In: *The Seismic Record* 4.3, pp. 161–171. DOI: https://doi.org/10.1785/0320240019.

Hudson, Thomas Samuel, Tom Kettlety, John-Michael Kendall, Tom O'Toole, Andrew Jupe, Robin K. Shail, and Augusta Grand (July 2024b). "Seismic Node Arrays for Enhanced Understanding and Monitoring of Geothermal Systems". In: *The Seismic Record* 4.3, pp. 161–171. ISSN: 2694-4006. DOI: https://doi.org/10.1785/032 0240019.

Hunter, J. D. (2007). "Matplotlib: A 2D graphics environment". In: *Computing in Science & Engineering* 9.3, pp. 90–95. DOI: 10.1109/MCSE.2007.55.

Hurd, Owen and Marco Bohnhoff (2012). "Stress-and structure-induced shear-wave anisotropy along the 1999 Izmit rupture, Northwest Turkey". In: *Bulletin of the Seismological Society of America* 102.5, pp. 2177–2188. DOI: https://doi.org/1 0.1785/0120110270.

Igonin, Nadine, James P. Verdon, and David W. Eaton (Mar. 2022). "Seismic Anisotropy Reveals Stress Changes around a Fault as It Is Activated by Hydraulic Fracturing". In: *Seismological Research Letters* 93.3, pp. 1737–1752. ISSN: 0895-0695. DOI: https://doi.org/10.1785/0220210282.

Illsley-Kemp, Finnigan, Martha K Savage, Colin JN Wilson, and Stephen Bannister (2019). "Mapping stress and structure from subducting slab to magmatic rift: Crustal seismic anisotropy of the North Island, New Zealand". In: *Geochemistry, Geophysics, Geosystems* 20.11, pp. 5038–5056. DOI: http://doi.org/10.1029/2019gc00852 9.

Jiang, Enyuan, Kelly H. Liu, Yuan Gao, Xiaofei Fu, and Stephen S. Gao (2021). "Spatial Variations of Upper Crustal Anisotropy Along the San Jacinto Fault Zone in Southern California: Constraints From Shear Wave Splitting Analysis". en. In: *Journal of Geophysical Research: Solid Earth* 126.4. _eprint:

https://onlinelibrary.wiley.com/doi/pdf/10.1029/2020JB020876, e2020JB020876. ISSN: 2169-9356. DOI: https://doi.org/10.1029/2020JB020876.

Jin, Zhaoyu, Mark Chapman, and Giorgos Papageorgiou (2018). "Frequency-dependent anisotropy in a partially saturated fractured rock". In: *Geophysical Journal International* 215.3, pp. 1985–1998. ISSN: 0956-540X. DOI: https://doi.org/10.1093/gji/ggy399.

Johnson, Jessica H., Martha K. Savage, and John Townend (2011). "Distinguishing between stress-induced and structural anisotropy at Mount Ruapehu volcano, New Zealand". en. In: *Journal of Geophysical Research: Solid Earth* 116.B12. _eprint: https://onlinelibrary.wiley.com/doi/pdf/10.1029/2011JB008308. ISSN: 2156-2202. DOI: https://doi.org/10.1029/2011JB008308.

Kaven, J. O., S. H. Hickman, A. F. McGarr, and W. L. Ellsworth (June 2015). "Surface Monitoring of Microseismicity at the Decatur, Illinois, CO2 Sequestration Demonstration Site". In: *Seismological Research Letters* 86.4, pp. 1096–1101. ISSN: 0895-0695. DOI: https://doi.org/10.1785/0220150062.

Kendall, J-M, QJ Fisher, S Covey Crump, J Maddock, A Carter, SA Hall, J Wookey, SLA Valcke, M Casey, G Lloyd, et al. (2007). "Seismic anisotropy as an indicator of reservoir quality in siliciclastic rocks". In: *Geological Society, London, Special Publications* 292.1, pp. 123–136. DOI: https://doi.org/10.1144/SP292.7.

Kendall, Michael, Toshiko Terakawa, Martha Savage, Tom Kettlety, Daniel Minifie, Haruhisa Nakamichi, and Andreas Wuestefeld (Apr. 2025). "Changes in seismic anisotropy at Ontake volcano: a tale of two eruptions". en. In: *Seismica* 4.1. Number: 1. ISSN: 2816-9387. DOI: https://doi.org/10.26443/seismica.v4i1.1101.

Kettlety, Tom, James P Verdon, Antony Butcher, Matthew Hampson, and Lucy Craddock (2020). "High-Resolution Imaging of the ML 2.9 August 2019 Earthquake in Lancashire, United Kingdom, Induced by Hydraulic Fracturing during Preston New Road PNR-2 Operations". In: *Seismological Research Letters* 92.1, pp. 151–169. ISSN: 0895-0695. DOI: https://doi.org/10.1785/0220200187.

Kettlety, Tom et al. (May 2024). "A Unified Earthquake Catalogue for the North Sea to Derisk European CCS Operations". en. In: *First Break* 42.5, pp. 31–36. ISSN: 0263-5046, 1365-2397. DOI: https://doi.org/10.3997/1365-2397.fb2024036.

Kingdon, Andrew, Mark W. Fellgett, and John D. O. Williams (2016). "Use of borehole imaging to improve understanding of the in-situ stress orientation of Central and Northern England and its implications for unconventional hydrocarbon resources". In: *Marine and Petroleum Geology* 73, pp. 1–20. ISSN: 0264-8172. DOI: `https://doi.org/10.1016/j.marpetgeo.2016.02.012`.

Kingdon, Andrew, John Williams, Mark Fellgett, Naomi Rettelbach, and Oliver Heidbach (2022). *Stress Map of Great Britain and Ireland 2022*. DOI: `http://doi.org/10.5880/WSM.GreatBritainIreland2022`.

Klein, RJ and MV Barr (Sept. 1986). "Regional state of stress in western Europe". In: *Proceedings of the International Symposium on Rock Stress and Rock Stress Measurements, Stockholm*. Ed. by O Stephansson. ISRM. Centek, Lulea, pp. 33–44.

Kufner, S.-K., J. Wookey, A. M. Brisbourne, C. Martín, T. S. Hudson, J. M. Kendall, and A. M. Smith (2023). "Strongly Depth-Dependent Ice Fabric in a Fast-Flowing Antarctic Ice Stream Revealed With Icequake Observations". en. In: *Journal of Geophysical Research: Earth Surface* 128.3. ISSN: 2169-9011. DOI: `https://doi.org/10.1029/2022JF006853`.

Link, Frederik and Maureen D. Long (Mar. 1, 2024). "SItomo – A toolbox for splitting intensity tomography and application in the Eastern Alps". In: *Journal of Geodynamics* 159, p. 102018. ISSN: 0264-3707. DOI: `https://doi.org/10.1016/j.jog.2024.102018`.

Liu, Sha, Stuart Crampin, Richard Luckett, and Jiansi Yang (Oct. 2014). "Changes in shear wave splitting before the 2010 Eyjafjallajökull eruption in Iceland". In: *Geophysical Journal International* 199.1, pp. 102–112. ISSN: 0956-540X. DOI: `https://doi.org/10.1093/gji/ggu202`.

Liu, Yun, Stuart Crampin, and Ian Main (1997). "Shear-wave anisotropy: spatial and temporal variations in time delays at Parkfield, Central California". In: *Geophysical Journal International* 130.3, pp. 771–785. DOI: `https://doi.org/10.1111/j.1365-246X.1997.tb01872.x`.

Lynner, Colton, Cherilyn Toro-Acosta, Eve Paulson, and Andrew Birkey (June 2024). "Local-S shear wave splitting along the length of the Alaska–Aleutian subduction

zone". In: *Geophysical Journal International* 237.3, pp. 1567–1574. ISSN: 1365-246X. DOI: https://doi.org/10.1093/gji/ggae107.

Matcham, I., M. K. Savage, and K. R. Gledhill (Jan. 2000). "Distribution of seismic anisotropy in the subduction zone beneath the Wellington region, New Zealand". In: *Geophysical Journal International* 140.1, pp. 1–10. ISSN: 0956-540X. DOI: https://doi.org/10.1046/j.1365-246x.2000.00928.x.

Nishiwaki, Takafumi, Aiming Lin, and Weiren Lin (2018). "Recovery of Stress During the Interseismic Period Around the Seismogenic Fault of the 1995 Mw 6.9 Kobe Earthquake, Japan". In: *Geophysical Research Letters* 45.23, pp. 12, 814–12, 820. DOI: https://doi.org/10.1029/2018GL079317.

Nur, Amos and Gene Simmons (Dec. 1969). "Stress-induced velocity anisotropy in rock: An experimental study". en. In: *Journal of Geophysical Research* 74.27, pp. 6667–6674. ISSN: 01480227. DOI: https://doi.org/10.1029/JB074i027p06667.

Nuttli, Otto (1961). "The effect of the Earth's surface on the S wave particle motion". In: *Bulletin of the Seismological Society of America* 51.2, pp. 237–246. DOI: https://doi.org/10.1785/BSSA0510020237.

Okada, Tomomi et al. (Feb. 2024). "Shear wave splitting and seismic velocity structure in the focal area of the earthquake swarm and their relation with earthquake swarm activity in the Noto Peninsula, central Japan". en. In: *Earth, Planets and Space* 76.1, p. 24. ISSN: 1880-5981. DOI: https://doi.org/10.1186/s40623-024-01974-0.

Okaya, David, Nikolas I. Christensen, Zachary E. Ross, and Francis T. Wu (2016). "Terrane-controlled crustal shear wave splitting in Taiwan". en. In: *Geophysical Research Letters* 43.2. _eprint: https://onlinelibrary.wiley.com/doi/pdf/10.1002/2015GL066446, pp. 556–563. ISSN: 1944-8007. DOI: https://doi.org/10.1002/2015GL066446.

OpenStreetMap contributors (2017). *Planet dump retrieved from https://planet.osm.org*. https://www.openstreetmap.org.

Pastori, M., P. Baccheschi, and L. Margheriti (Sept. 2019). "Shear Wave Splitting Evidence and Relations With Stress Field and Major Faults From the "Amatrice-Visso-Norcia Seismic Sequence"". en. In: *Tectonics* 38.9, pp. 3351–3372. ISSN: 0278-7407, 1944-9194. DOI: https://doi.org/10.1029/2018TC005478.

Plumb, Richard A. and Stephen H. Hickman (1985). "Stress-induced borehole elongation: A comparison between the four-arm dipmeter and the borehole televiewer in the Auburn Geothermal Well". In: *Journal of Geophysical Research: Solid Earth* 90.B7, pp. 5513–5521. DOI: https://doi.org/10.1029/JB090iB07p05513.

Reiss, Miriam Christina and Georg Rümpker (2017). "SplitRacer: MATLAB Code and GUI for Semiautomated Analysis and Interpretation of Teleseismic Shear-Wave Splitting". In: *Seismological Research Letters* 88.2A, pp. 392–409. ISSN: 0895-0695. DOI: https://doi.org/10.1785/0220160191.

Savage, M. K., A. Wessel, N. A. Teanby, and A. W. Hurst (2010a). "Automatic measurement of shear wave splitting and applications to time varying anisotropy at Mount Ruapehu volcano, New Zealand". In: *Journal of Geophysical Research: Solid Earth* 115.B12. DOI: https://doi.org/10.1029/2010JB007722.

Savage, Martha K, Takao Ohminato, Yosuke Aoki, Hiroshi Tsuji, and Sonja M Greve (2010b). "Stress magnitude and its temporal variation at Mt. Asama Volcano, Japan, from seismic anisotropy and GPS". In: *Earth and Planetary Science Letters* 290.3-4, pp. 403–414. DOI: https://doi-org/10.1016/j.epsl.2009.12.037.

Seher, T. and I. G. Main (Apr. 2004). "A statistical evaluation of a 'stress-forecast' earthquake". In: *Geophysical Journal International* 157.1, pp. 187–193. ISSN: 0956-540X. DOI: https://doi.org/10.1111/j.1365-246X.2004.02186.x.

Silver, Paul G and W Winston Chan (1991). "Shear wave splitting and subcontinental mantle deformation". In: *Journal of Geophysical Research: Solid Earth* 96.B10, pp. 16429–16454. DOI: https://doi.org/10.1029/91jb00899.

Skurtveit, Elin et al. (2022). "Improved quantification of CO2 storage containment risks — an overview of the SHARP Storage project". In: *16th Greenhouse Gas Control Technologies Conference 2022 (GHGT-16)*. 16th International Conference on Greenhouse Gas Control Technologies, Lyon, France, 23–27 Oct 2022. SSRN – Social Science Research Network.

Spingos, Ioannis, Vasilis Kapetanidis, Georgios Michas, George Kaviris, and Filippos Vallianatos (June 2023). "Shear-wave splitting patterns in Perachora (Eastern Gulf of Corinth, Greece)". en. In: *Annals of Geophysics* 66.2. Number: 2, SE209–SE209. ISSN: 2037-416X. DOI: https://doi.org/10.4401/ag-8829.

Spingos, Ioannis, George Kaviris, Christos Millas, Panayotis Papadimitriou, and Nicholas Voulgaris (Jan. 2020). "Pytheas: An open-source software solution for local shear-wave splitting studies". In: *Computers & Geosciences* 134, p. 104346. ISSN: 0098-3004. DOI: https://doi.org/10.1016/j.cageo.2019.104346.

Stork, Anna L., James P. Verdon, and J.-Michael Kendall (Jan. 2015). "The microseismic response at the In Salah Carbon Capture and Storage (CCS) site". In: *International Journal of Greenhouse Gas Control* 32, pp. 159–171. ISSN: 1750-5836. DOI: https://doi.org/10.1016/j.ijggc.2014.11.014.

Survey, British Geological (2021). *BGS Geology 625k Faults Dataset.* https://ogcapi.bgs.ac.uk/collections/BGSGeology625kFaults. Accessed 26 June 2025.

Teanby, N., J.-M. Kendall, R. H. Jones, and O. Barkved (Mar. 2004a). "Stress-induced temporal variations in seismic anisotropy observed in microseismic data". In: *Geophysical Journal International* 156.3. _eprint: https://academic.oup.com/gji/article-pdf/156/3/459/5883127/156-3-459.pdf, pp. 459–466. ISSN: 0956-540X. DOI: https://doi.org/10.1111/j.1365-246X.2004.02212.x.

Teanby, Nicholas A, J-M Kendall, and M Van der Baan (2004b). "Automation of shear-wave splitting measurements using cluster analysis". In: *Bulletin of the Seismological Society of America* 94.2, pp. 453–463. DOI: https://doi.org/10.1785/0120030123.

Uieda, Leonardo, Dongdong Tian, Wei Ji Leong, Liam Toney, Michael Grund, Jack T. Williams, Megan Jones, William Schlitzer, Jonas de Souza, and Paul Wessel (2021). "PyGMT: A Python interface for the Generic Mapping Tools". In: *The Journal of Open Source Software* 6.64, p. 3488. DOI: 10.21105/joss.03488.

Verdon, J. P., J.-M. Kendall, and Andreas Wüstefeld (2009). "Imaging fractures and sedimentary fabrics using shear wave splitting measurements made on passive seismic data". In: *Geophysical Journal International* 179.2. Publisher: Blackwell Publishing Ltd Oxford, UK, pp. 1245–1254. DOI: https://doi.org/10.1111/j.1365-246X.2009.04347.x.

Verdon, James P and J-Michael Kendall (2011). "Detection of multiple fracture sets using observations of shear-wave splitting in microseismic data". In: *Geophysical*

Prospecting 59.4, pp. 593–608. DOI: `https://doi.org/10.1111/j.1365-2478.2010.00943.x`.

Verdon, James P., J. -Michael Kendall, Anna C. Horleston, and Anna L. Stork (Nov. 2016). "Subsurface fluid injection and induced seismicity in southeast Saskatchewan". In: *International Journal of Greenhouse Gas Control* 54, pp. 429–440. ISSN: 1750-5836. DOI: `https://doi.org/10.1016/j.ijggc.2016.04.007`.

Volti, T and S Crampin (2003). "A four-year study of shear-wave splitting in Iceland: 2. Temporal changes before earthquakes and volcanic eruptions". In: *Geological Society, London, Special Publications* 212.1, pp. 135–149. DOI: `https://doi.org/10.1144/GSL.SP.2003.212.01.09`.

Walsh, E., R. Arnold, and M. K. Savage (Oct. 2013). "Silver and Chan revisited". In: *Journal of Geophysical Research: Solid Earth* 118.10, pp. 5500–5515. ISSN: 21699313. DOI: `https://doi.org/10.1002/jgrb.50386`.

Wookey, James (2012). "Direct probabilistic inversion of shear wave data for seismic anisotropy". In: *Geophysical Journal International* 189.2, pp. 1025–1037. ISSN: 0956540X. DOI: `https://doi.org/10.1111/j.1365-246x.2012.05405.x`.

Wuestefeld, Andreas, Othman Al-Harrasi, James P Verdon, James Wookey, and J Michael Kendall (2010). "A strategy for automated analysis of passive microseismic data to image seismic anisotropy and fracture characteristics". In: *Geophysical Prospecting* 58.5, pp. 755–773. DOI: `https://doi.org/10.1111/j.1365-2478.2010.00891.x`.

Wüstefeld, Andreas, Götz Bokelmann, Christophe Zaroli, and Guilhem Barruol (May 2008). "SplitLab: A shear-wave splitting environment in Matlab". In: *Computers & Geosciences* 34.5, pp. 515–528. ISSN: 0098-3004. DOI: `https://doi.org/10.1016/j.cageo.2007.08.002`.

Zatsepin, Sergei V. and Stuart Crampin (1997). "Modelling the compliance of crustal rock—I. Response of shear-wave splitting to differential stress". In: *Geophysical Journal International* 129.3, pp. 477–494. ISSN: 1365-246X. DOI: `https://doi.org/10.1111/j.1365-246x.1997.tb04488.x`.